Chapter Four

Kinetic and Thermodynamic Approaches for the Synthesis of Ammonium Ion/Crown Ether-Based Interlocked Molecules

"It's the end of the world as we know it, and I feel fine"
– R.E.M.

The research described in this **Chapter** is based upon three publications:

Cantrill, S. J.; Fulton, D. A.; Fyfe, M. C. T.; Stoddart, J. F.; White, A. J. P.; Williams, D. J. *Tetrahedron Lett*. **1999**, *40*, 3669–3672.

Cantrill, S. J.; Rowan, S. J.; Stoddart, J. F. *Org. Lett.* **1999**, *1*, 1363–1366.

Cantrill, S. J.; Fulton, D. A.; Heiss, A. M.; Pease, A. R.; Stoddart, J. F.; White, A. J. P.; Williams, D. J. *Chem. Eur. J.* **2000**, *6*, 2274–2287.

Table of Contents

Abstract: The reaction between amino and isocyanate groups has been exploited for the synthesis—under kinetic control—of both dibenzo[24]crown-8- and benzometaphenylene[25]crown-8-containing ureido-[2]rotaxanes, the latter of which represents the first example of an interlocked structure incorporating this particular crown ether. Both [2]rotaxanes have been fully characterized by ^{1}H and ^{13}C NMR spectroscopies, FAB mass spectrometry and X-ray crystallography. Interestingly, the unsymmetrical nature of the dumbbell-shaped component in each of the two [2]rotaxanes renders each face of the encircling macrocyclic polyether diastereotopic, a feature that is apparent upon inspection of their ^{1}H NMR spectra. In contrast, thermodynamic control can also be exploited in the synthesis of a [2]rotaxane based upon the dibenzylammonium ion/crown ether recognition motif. When dibenzo[24]crown-8 (DB24C8) is added to an acetonitrile solution containing a diimine dumbbell-like component, the dynamic nature of the system (*i.e.*, imine hydrolysis/reformation) offers the ring component access to the NH_2^+ center, allowing the self-assembly of the corresponding 'dynamic' [2]rotaxane to occur. Furthermore, the 'fixing' of this [2]rotaxane can be achieved upon reduction of the imine bonds, affording a kinetically-inert [2]rotaxane.

4.1. Introduction

Interlocked molecules[1] are comprised of two or more mechanically-linked components between which no covalent bonds exist. Catenanes[2] and rotaxanes[3] (Figure 4.1) are the most common examples of such compounds, but more exotic structures have been postulated[4] and indeed synthesized.[5] Perhaps dismissed as chemical curiosities in their infancy, interlocked molecules are now making their own headlines.[6] New generations of these compounds are emerging[7]—alongside more traditional non-interlocked counterparts—as prototypical molecular machines.[8] Indeed, ingenious nano-sized devices[9] with characteristics akin to motors[10] and switches[11] have all been realized, the latter of which potentially heralds the arrival of molecular computing.[6,12] The considerable impact of such 'curious' molecules in today's technologically-driven

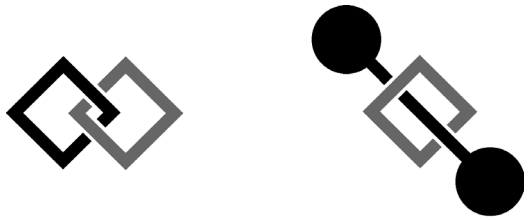

Figure 4.1. A schematic representation of the generic structures of the two most widely studied classes of interlocked molecules.

society has undoubtedly spurred efforts to optimize their syntheses. Accordingly, this new found impetus has not only made interlocked compounds much more accessible, but has increased their structural diversity dramatically.

4.1.1. Threading, Clipping, and Slipping: How to Make Interlocked Molecules

Synthetic approaches to the syntheses of interlocked compounds have evolved tremendously since the first synthesis of a [2]catenane was reported[13] in 1960. Nonetheless, at a conceptual level, the syntheses of all interlocked molecules are fundamentally very similar. In order to achieve *efficient* interlocking, the precursors of the components—*i.e.,* those that will ultimately constitute the target structure—must be held in close proximity whilst also being disposed in a very precise manner relative to one another, immediately prior to a final post-assembly modification step. Consequently, the early 'statistical' strategies—relying simply upon chance to bring the necessary components into the correct geometry required for the formation of an interlocked molecule—resulted in very poor yields of the desired interlocked products. However, these demanding spatial requirements *can* be satisfied by either (i) employing a temporary covalent scaffold to which the precursors are linked initially, or (ii) utilizing self-assembly[14] processes to generate the necessary *threaded* or *entwined* complexes. The former approach, *i.e.*, covalent templating,[15] surpassed the statistical method, but the syntheses—although undoubtedly elegant—were both demanding and time-consuming. Ultimately, it was the latter approach—built upon the principles of supramolecular chemistry[16]—that superceded all earlier protocols, exploiting delicate noncovalent

interactions to create complexes in which the correct orientation of (pre)components is achieved. Subsequent modification of such complexes *via* covalent (or coordinative) bond formation can lead to the construction of interlocked species. For example, the synthesis (Figure 4.2) of a [2]catenane requires (i) the formation of a *threaded* complex[17] followed

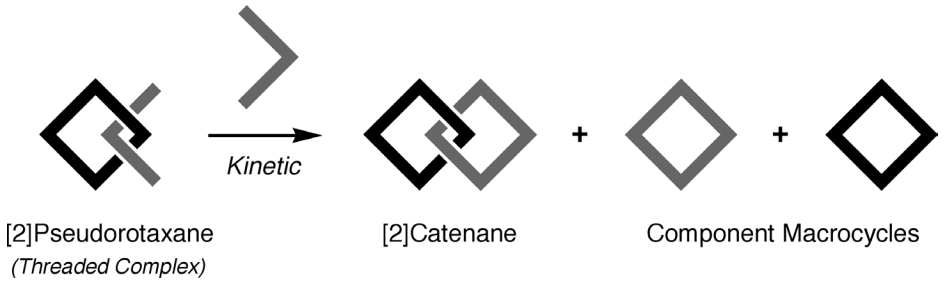

Figure 4.2. A schematic representation depicting the kinetic synthesis of a [2]catenane from the appropriate [2]pseudorotaxane.

by (ii) the linking of the ends of the thread component.[18] The same *threaded* complex can also be utilized[19] in the synthesis (Figure 4.3a) of a [2]rotaxane—employing a '*stoppering*' methodology—whereupon the ends of the thread are capped with bulky

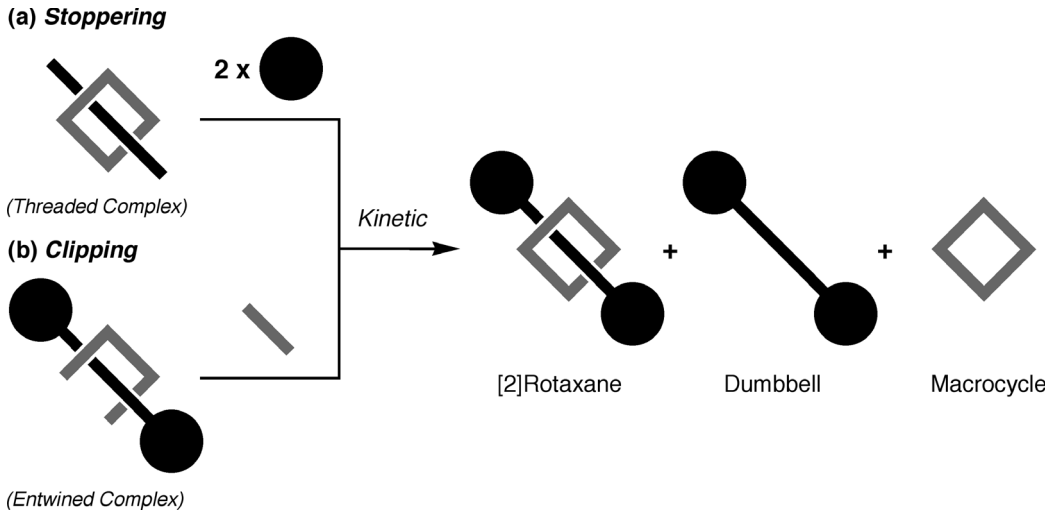

Figure 4.3. Both (**a**) stoppering, and (**b**) clipping approaches can be utilized for the synthesis—performed under kinetic control—of a [2]rotaxane.

groups over which the ring component cannot pass. One alternative approach (Figure 4.3b) to rotaxane synthesis—the '*clipping*' method—involves the participation of an *entwined* complex formed between two acyclic components.[20] In this case, the macrocycle is fabricated around the preformed dumbbell-shaped component. Finally, often touted[21] as the third—and most recently developed[22]—strategy for producing rotaxanes, '*slippage*' completes the synthetic repertoire.

The '*slippage*' approach (Figure 4.4) is, at least initially, very similar to that of *stoppering*, *i.e.*, each protocol demands the threading of a linear component through the cavity of a macrocyclic one. Subsequently, however, whereas *stoppering* requires bond formation to create a kinetically-stable compound (a rotaxane), *slippage* relies upon subtle manipulation of the complexation and de-complexation rates in order to confer kinetic stability upon its products (pseudorotaxanes). The size of the linear component's end-groups—in relation to the dimensions of the macroring's aperture—influences the rates at which a [2]pseudorotaxane is assembled/disassembled. Therefore, the judicious choice[23] of a *slippage* 'stopper', complementary to a particularly-sized macrocycle, can result in a situation where—over an easily accessible temperature range—the kinetics of threading/dethreading vary significantly. The extent of this kinetic disparity can be

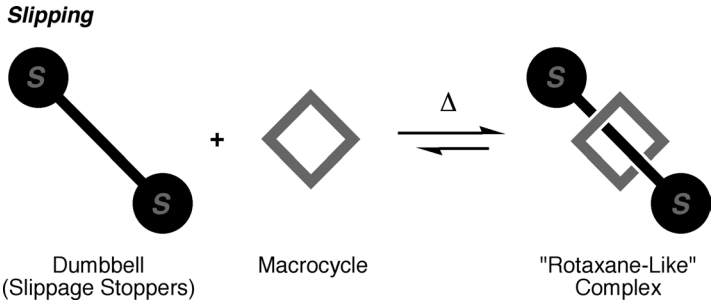

Figure 4.4. The slippage synthesis of a 'rotaxane-like' complex relies upon the precise matching of the end groups of the dumbbell and the size of the cavity of the macroring through which the dumbbell has to pass.

utilized[24,25] to thread a ring component onto a *slippage* 'stopper'-capped dumbbell at one temperature, but essentially prevent its passage—as a consequence of extraordinarily slow kinetics—at another, lower, temperature. Hence, heating up a solution containing two such kindred components permits the thermodynamic equilibrium to be reached, which, if in favor of [2]pseudorotaxane formation, will result, upon subsequent cooling down of the solution, in a kinetically-stable [2]pseudorotaxane. However, the utility of this approach is tempered by the fact that the products are not rotaxanes, but merely pseudorotaxanes (or 'rotaxane-like complexes')[25] that are stable only under certain environmental conditions – an increase in temperature, solvent polarity and acidity all having profound—often deleterious—consequences upon pseudorotaxane stability.

4.1.2. Kinetic and Thermodynamic Considerations

To date, the final post-assembly modification steps employed[1] in the majority of interlocked molecule syntheses have been performed under *kinetic* control. Consequently, such strategies can result (Figures 4.2 and 4.3) in the irreversible formation of undesired—non-interlocked—products, thereby potentially reducing the efficiency of these processes. In contrast, however, a reversible *thermodynamically*-controlled approach allows for a 'proof-reading' step in which 'incorrect' structures

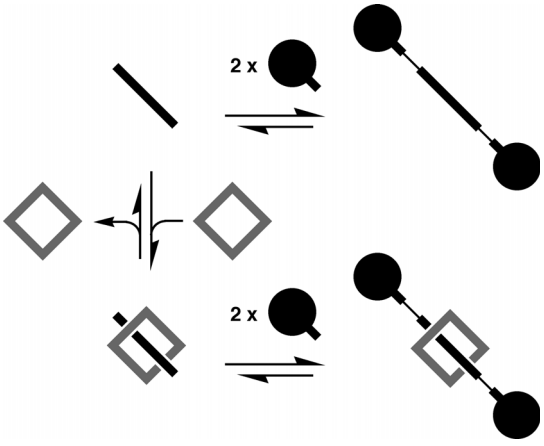

Figure 4.5. A schematic representation depicting the thermodynamically-controlled synthesis of a [2]rotaxane using the 'stoppering' methodology. Note: the thinner lines represent the reversibly-formed covalent bonds; a convention that will be used throughout the remainder of this Chapter.

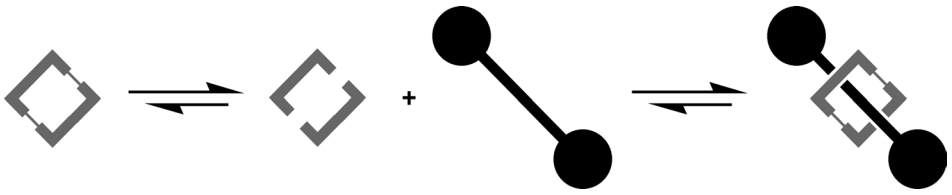

Figure 4.6. A schematic representation depicting the thermodynamically-controlled synthesis of a dynamic [2]rotaxane utilizing 'clipping' methodology.

are consumed and their component parts recycled back into an equilibrating mixture. For example, in a stoppering reaction performed (Figure 4.5) under reversible conditions, the formation of a dumbbell-shaped component (top right) does not represent a dead end, as it would if this reaction was performed under kinetic control (*vide supra*). In this case, such an undesired structure can simply re-equilibrate, and its components can go on to form the desired dynamic [2]rotaxane product (bottom right). Furthermore, thermodynamic approaches for the syntheses of interlocked molecules are, however, not limited to stoppering reactions. The thermodynamically-controlled clipping (Figure 4.6) of a macrocyclic component around a preformed dumbbell-shaped molecule can also be envisaged. In fact, there are many ways *via* which dynamic [2]catenanes and [2]rotaxanes can be assembled, depending upon whether just one, or both of the components possess (Figure 4.7), within their framework, bonds that can be made and broken

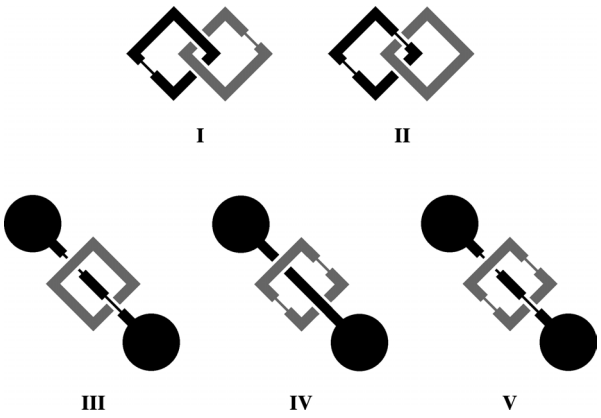

Figure 4.7. Schematic representations of dynamic interlocked structures (catenanes **I**-**II** and rotaxanes **III**-**V**) which differ in the location of the reversible covalent bonds. For example, whereas the dumbbell of **III** can be formed and broken reversibily, it is the ring component of **IV** that contains the reversible covalent bonds. Consequently, dynamic rotaxane **III** would be formed by a 'stoppering' approach, whereas **IV** would required a clipping strategy. Rotaxane **V**, in which both components contain reversibly-formed linkages, could be assembled *via* either pathway.

reversibily. Additionally, the possibility exists for interlocked molecules to be assembled (Figure 4.8) directly from their constituent components. For example, by mixing two preformed macrocycles with one another—at least one of which contains a reversibily-formed bond—it is possible, under the appropriate conditions, to reproduce the conjurer's 'magic rings' trick, wherein two apparently 'closed' rings can be linked together, one through the other, to form a [2]catenane. The corresponding process for rotaxanes, has been referred to[26] as the 'magic rods' trick. Synthetic chemists are already exploring the opportunities presented by utilizing reversible bond-forming reactions, in conjunction with supramolecular assistance,[27] to make molecular receptors[28] and interlocked molecules, such as catenanes and rotaxanes. To date, labile coordinative bonds, associated with certain metal-ligand interactions[29] and ring-opening/ring-closing metathesis protocols,[30] have been exploited in the self-assembly of catenanes under thermodynamically-controlled conditions. In addition, a wide range of functionalities, including acetals,[31] esters,[32] disulfides,[33] hydrazones,[34] anhydrides of hydroxy-borazaaromatics,[35] and oximes,[36] have also been employed in reversible processes involving wholly organic compounds.

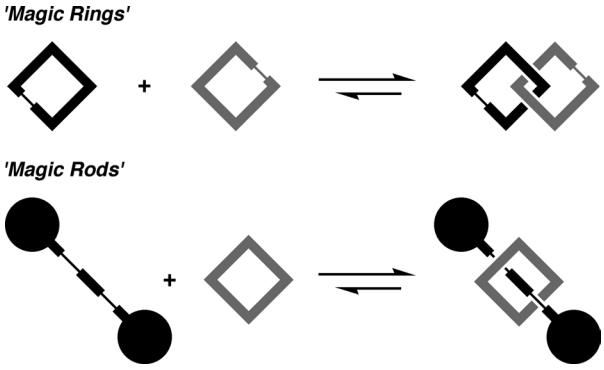

Figure 4.8. Schematic representations of 'magic' interlocked molecules!

This Chapter focuses upon the synthesis of [2]rotaxanes—based upon crown ether/secondary ammonium ion recognition—using both kinetic and thermodynamic strategies. Initially, a kinetic approach is explored, in which the reaction between amino

and isocyanate groups results in the formation of ureido-[2]rotaxanes. Subsequently, the reversible formation of imine bonds, is exploited for the synthesis—under thermodynamic control—of a dynamic [2]rotaxane.

4.2. A Kinetic Approach – Urea Formation

Reactions performed on supramolecular assemblies based upon secondary ammonium ion/crown ether recognition—*e.g.*, for the purposes of forming interlocked molecules—can only be carried out under a certain set of conditions. Strongly basic conditions cannot be employed, as such approaches would result in deprotonation of the secondary ammonium ion, thereby destroying any molecular recognition. Furthermore, the magnitude of the interaction between ammonium ions and crown ethers is significantly reduced, (i) at elevated temperatures[37] and, (ii) in highly polar solvents[38] (*e.g.*, DMSO, H_2O, DMF), and thus reactions requiring high temperatures or polar solvents must also be avoided. Based upon these criteria, therefore, the facile reaction between amino and isocyanate groups was investigated for the purposes of kinetically-trapping an ammonium ion/crown ether assembly to form a [2]rotaxane. A linear secondary ammonium ion containing molecule—possessing, at one end, a bulky stopper group and, at the other end, an amino group—was mixed[39] (Figure 4.9) with a complementary crown

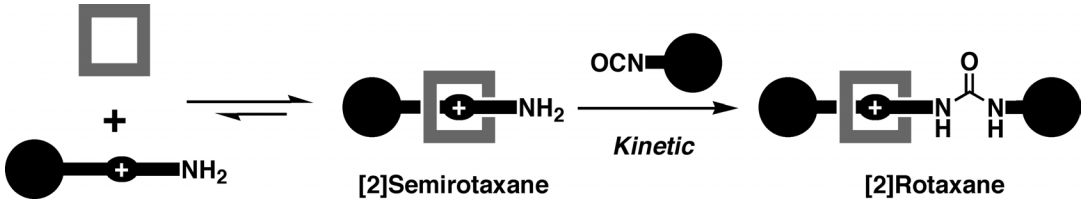

Figure 4.9. Conceptually, the assembly of an amino-functionalized [2]semirotaxane and subsequent reaction with a bulky isocyanate leads to the formation of a ureido-[2]rotaxane.

ether component (either DB24C8 or BMP25C8), and reacted with a bulky isocyante to afford a ureido-[2]rotaxane.

4.2.1. A DB24C8-Containing [2]Rotaxane

The template-directed synthesis of the [2]rotaxane **1**-H·O_2CCF_3 is illustrated in Scheme 4.1. 4-Aminobenzyl-3,5-di-*t*-butylbenzylamine (**4**) was prepared by $NaBH_4$ reduction of

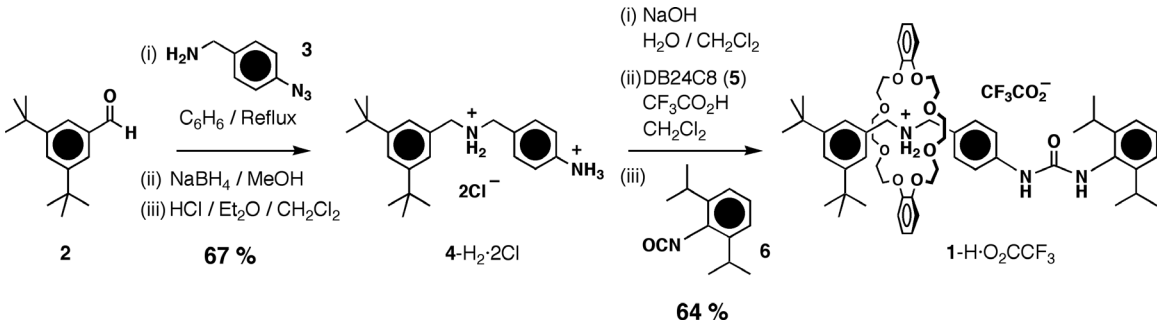

Scheme 4.1. The synthesis of the [2]rotaxane **1**-H·O_2CCF_3.

the imine generated from the condensation of 3,5-di-*t*-butylbenzaldehyde[40] (**2**) and 4-azidobenzylamine[41] (**3**). It was isolated as its dihydrochloride salt **4**-H_2·2Cl in an overall yield of 67 %. Deprotonation of this salt was followed by the addition of one equivalent of CF_3CO_2H which presumably brought about the monoprotonation of the diamine **4** at the more basic secondary dibenzylamine site. As a consequence, an $R_2NH_2^+$ ion is generated which is capable of recognizing the DB24C8 (**5**) molecules also present in the solution. Addition of 2,6-diisopropylphenylisocyanate (**6**), followed by work-up and subsequent chromatographic purification, afforded the [2]rotaxane **1**-H·O_2CCF_3 as the major product in a 64 % yield.

NMR Spectroscopy

The full assignment of the ^{1}H NMR spectrum and in-depth analysis of the ^{13}C NMR spectrum (see Section 4.5) was made possible by two-dimensional ^{1}H-^{1}H correlation (COSY) and ^{1}H-^{13}C correlation (HMQC) experiments. The unsymmetrical nature of the dumbbell-shaped component of the [2]rotaxane **1**-H·O_2CCF_3 renders the protons on each face of the encircling macrocycle heterotopic (Figure 4.10). When a symmetrical thread/dumbbell is bound/encircled by a DB24C8 macroring, the resonances associated with the α- and β-OCH_2 protons of the crown ether appear as narrow multiplets, and the resonance of the γ-OCH_2 protons gives rise to a singlet. In the case of **1**-H·O_2CCF_3, there are now two distinct environments for each of these pairs of protons, respectively, *i.e.*, the protons (α^1, β^1 and γ^1) on the side of the macrocycle facing toward the 3,5-di-*t*-butylphenyl stopper are different from those (α^2, β^2 and γ^2) facing the 2,6-diisopropylphenyl stopper on the other side of the macrocycle. The facial desymmetrization of the crown ether is evident and has a profound effect upon the ^{1}H NMR spectrum (Figure 4.11) of this compound.

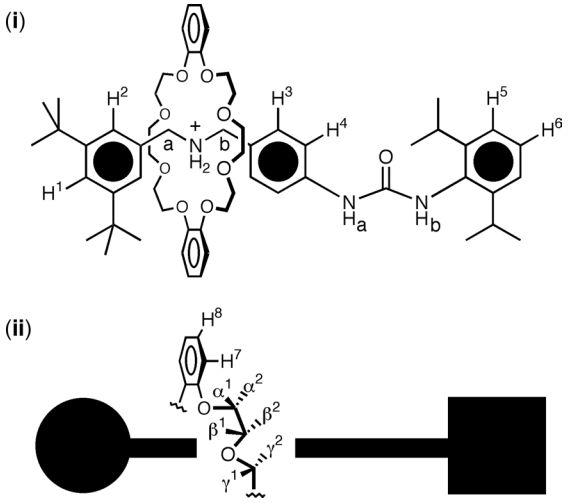

Figure 4.10. The structure of the [2]rotaxane **1**-H·O_2CCF_3, showing the labeling scheme for both (**i**) the dumbbell and (**ii**) the crown ether components, used in describing its NMR spectroscopic properties. The schematic representation (**ii**) highlights the unsymmetrical nature of the dumbbell. The protons (α^1, β^1, γ^1) on one face of the DB24C8 macrocycle are oriented toward the 3,5-di-*tert*-butylphenyl stopper, whereas those protons (α^2, β^2, γ^2) on the opposite face of the macrocycle are directed toward the 2,6-diisopropylphenyl stopper, *i.e.,* the protons located on opposite faces of the crown ether are diastereotopic.

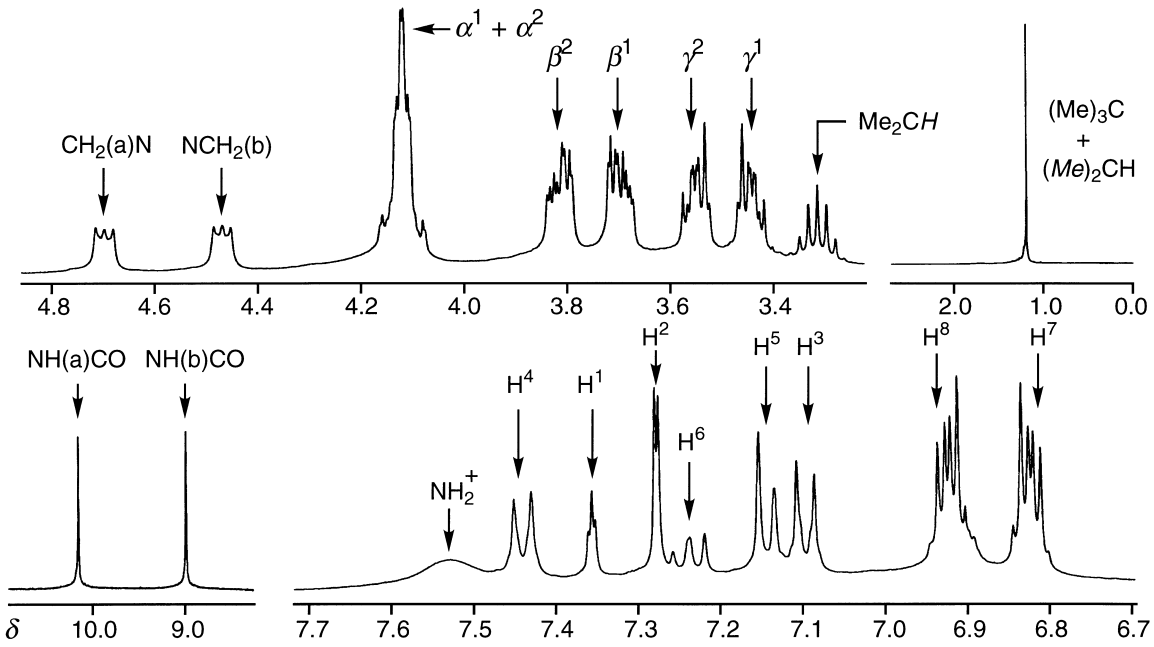

Figure 4.11. The partial ^{1}H NMR spectrum (400 MHz, CD_2Cl_2) of **1**-H·O_2CCF_3.

Although the resonances for the α-OCH_2 protons overlap, those associated with the β- and γ-OCH_2 protons are separated such that distinct multiplets are observed for β^1- and β^2-OCH_2 and γ^1- and γ^2-OCH_2 protons. The unambiguous assignment of the superscripts '1' and '2' (denoting the face of the macrocycle on which a particular proton resides) was made upon inspection of the T-ROESY spectrum. Two important probe protons on the dumbbell's backbone are H-2 and H-3. Should, as expected,[42] the DB24C8 macroring encircle the NH_2^+ center, in preference to the urea moiety, H-2 and H-3 will flank the macrocycle. Indeed, this hypothesis is confirmed upon inspection of the partial T-ROESY spectrum shown in Figure 4.12. Through-space interactions are observed[43] between H-2, on the dumbbell, and all of the OCH_2 protons (α^1, β^1 and γ^1) on only one side of the macrocycle. The corresponding pattern is observed for H-3, which only correlates to resonances arising from the α^2-, β^2- and γ^2-OCH_2 protons residing on the opposite face of the crown ether.

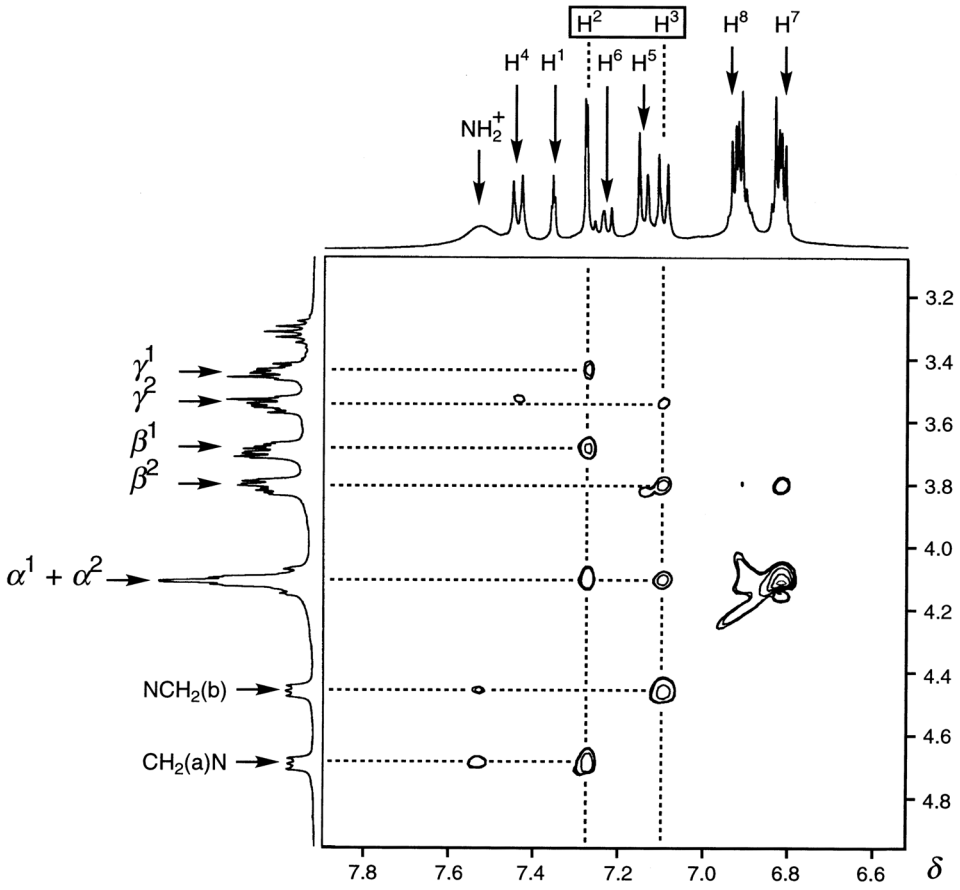

Figure 4.12. The partial T-ROESY spectrum (400 MHz, CD_2Cl_2) of **1**-H·O_2CCF_3. The most significant probe protons are H-2 and H-3, which each show a correlation to only one set of protons on only one face of the crown ether.

X-Ray Crystallography

Single crystals, suitable for X-ray crystallographic analysis, were obtained upon layering a CH_2Cl_2 solution of the [2]rotaxane **1**-H·O_2CCF_3 with hexanes. The X-ray crystal analysis of the [2]rotaxane shows the crystals to contain two independent molecules in the asymmetric unit. In both molecules, it is the NH_2^+ center that is encircled by the DB24C8 macrocycle with the urea component hydrogen bonded to the trifluoroacetate counterion. Stabilization in both independent molecules is *via* a combination of N–H^+···O

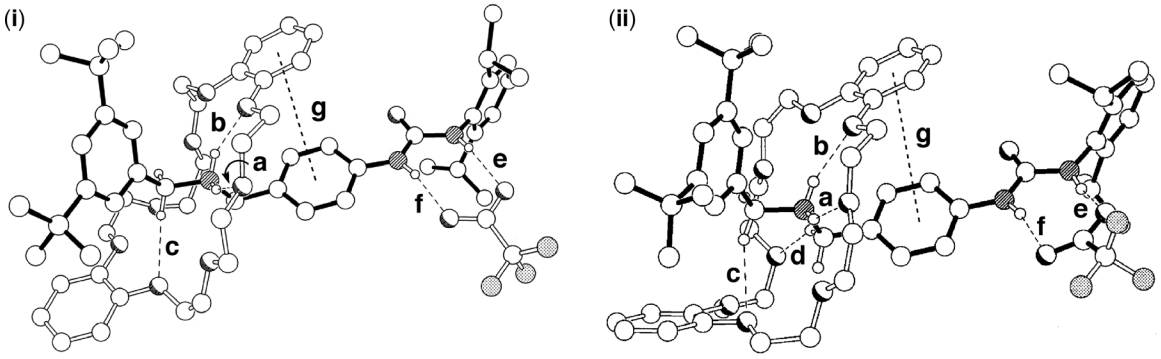

Figure 4.13. The molecular structures of the two crystallographically-independent [2]rotaxanes present in the crystals of **1**-H·O_2CCF_3. Hydrogen bonding distances and angles {[X···O], [H···O] distances (Å), [X–H···O] angles (°)}: for molecule (**i**); (**a**) 2.85, 2.01, 156; (**b**) 2.89, 2.16, 137; (**c**) 3.31, 2.36, 171; (**e**) 2.89, 2.03, 159; (**f**) 2.86, 1.98, 164; for molecule (**ii**); (**a**) 2.91, 2.11, 147; (**b**) 3.01, 2.23, 145; (**c**) 3.41, 2.51, 157; (**d**) 3.25, 2.41, 147; (**e**) 2.76, 1.92, 163; (f) 2.91, 2.02, 168. The centroid-centroid distances (**g**) for molecules (**i**) and (**ii**) are 4.48 and 4.54 Å, respectively.

and C–H···O hydrogen bonding interactions, as illustrated in Figure 4.13. The conformation of the cationic dumbbell in both molecules is essentially the same with the plane of the urea fragment steeply inclined to the plane of the terminal 2,6-diisopropylphenyl ring but lying close to the plane of the central *p*-toluidinyl ring (**w** and **x** in Table 4.1, respectively). The plane of the all-*anti* $CCH_2NH_2^+CH_2C$ backbone is steeply inclined to both the central *p*-toluidinyl and the 3,5-di-*t*-butylphenyl ring systems (**y** and **z** in Table 4.1, respectively). However, the conformations of the two independent

Table 4.1. The torsion angles (**w**, **x**, **y** and **z**) observed for the DB24C8- and BMP25C8-containing rotaxanes, **1**-H·O_2CCF_3 and **7**-H·O_2CCF_3, respectively. In each structure, there are two crystallographically-independent molecules (**i** and **ii**) in the asymmetric unit.

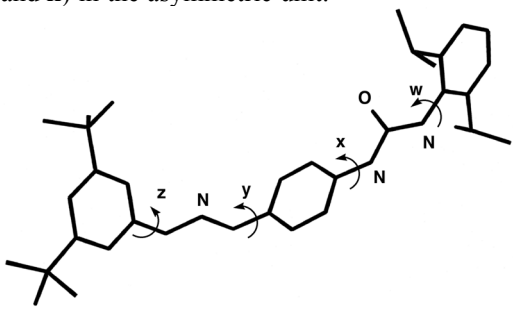

	Torsion Angles (°)			
Structure	**w**	**x**	**y**	**z**
{DB24C8 (**5**)}				
1-H·O_2CCF_3 (**i**)	84	10	86	64
1-H·O_2CCF_3 (**ii**)	70	16	85	63
{BMP25C8(**8**)}				
7-H·O_2CCF_3 (**i**)	72	4	75	59
7-H·O_2CCF_3 (**ii**)	90	3	86	54

DB24C8 macrocycles differ, both crown ethers having an extended geometry, but with distinctly different geometries for one of the polyether linkages. In both independent molecules, there is an apparent overlaying of one of the catechol rings and the *p*-toluidinyl ring of the cationic dumbbell. The centroid-centroid distances (4.48 Å in **i** and 4.54 Å in **ii**) are, however, too great for any significant intramolecular π–π stacking interactions. There is also a marked absence of any inter-[2]rotaxane interactions, although there is evidence for a weak intermolecular C–H···π interaction (H···π 2.73 Å, C–H···π angle 148°) between one of the methylene hydrogen atoms in one of the polyether chains in molecule **ii** and one of the catechol rings of a symmetry-related [2]rotaxane.

4.2.2. A BMP25C8-Containing [2]Rotaxane

Subsequently, in the knowledge that BMP25C8 (**8**) can accommodate an $R_2NH_2^+$ ion within its macrocyclic cavity, the construction of a [2]rotaxane incorporating this crown

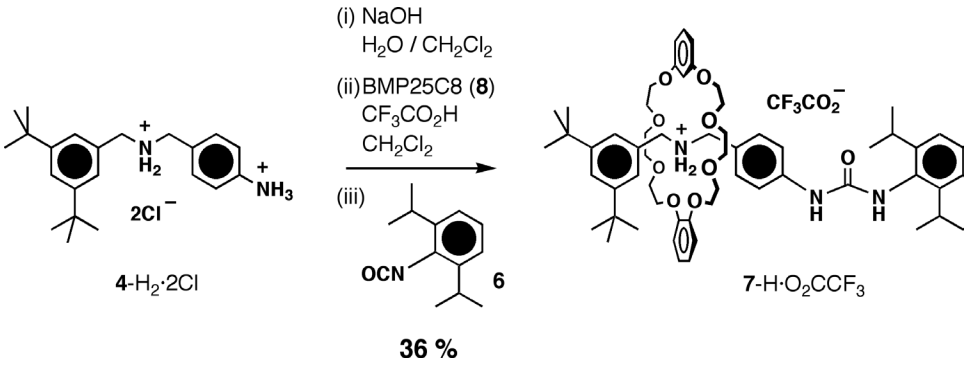

Scheme 4.2. The synthesis of the first BMP25C8-containing [2]rotaxane **7**-H·O_2CCF_3

ether[44] was the next goal. Employing the same methodology as that shown to work for DB24C8 (**5**), the BMP25C8-containing [2]rotaxane **7**-H·O_2CCF_3 was obtained (Scheme 4.2) in a 36 % yield.

NMR Spectroscopy

As in the case of the DB24C8-containing [2]rotaxane **1**-H·O_2CCF_3, the macrocyclic polyether component in **7**-H·O_2CCF_3 is also desymmetrized facially as a consequence of the unsymmetrical nature of the dumbbell-shaped component. A sharp well-resolved ^{1}H NMR spectrum (400 MHz, CD_2Cl_2) was obtained (Figure 4.14) for **7**-H·O_2CCF_3. The

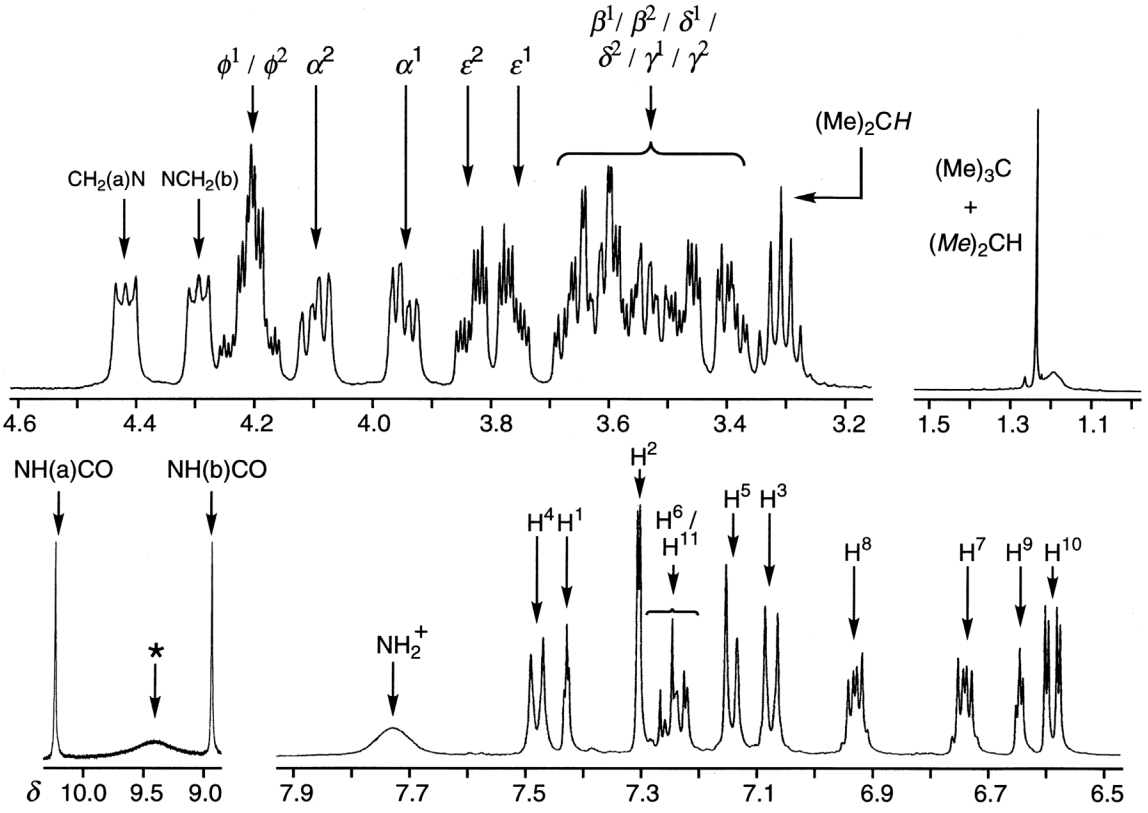

Figure 4.14. The partial ^{1}H NMR spectrum (400 MHz, CD_2Cl_2) of **7**-H·O_2CCF_3. Note (*) that the broad peak at δ = 9.4 ppm is a background signal arising from the NMR probe.

separation of the resonances arising from the crown ether's polyether protons is evident. Additionally, the spectroscopic characteristics of the BMP25C8 component are considerably more complex than those of DB24C8 on account of there being six sets of

chemically inequivalent OCH_2 groups (α, β, γ, δ, ε and ϕ) in each polyether arc in BMP25C8, as opposed to only three (α, β and γ) in the case of DB24C8. Once again, a combination of two-dimensional NMR techniques—namely, COSY, T-ROESY and HMQC experiments—permitted a complete interpretation of the ^1H NMR spectrum. Each unique face of the macrocycle could be distinguished by inspection of the T-ROESY spectrum, wherein, as before, the resonances arising from the highly diagnostic H-2 and H-3 protons of the dumbbell only correlated (Figure 4.15) with the resonances associated with the OCH_2 protons located on the side of the macrocyclic polyether facing them. Several through-space correlations were detected in the T-ROESY experiment: some of the more important ones are indicated in Figure 4.15. Perhaps the most notable interaction is that observed between the H-9 resonance—the isolated aromatic proton attached to the resorcinol ring present in the BMP25C8 component—and the two benzylic methylene groups adjacent to the NH_2^+ center of the

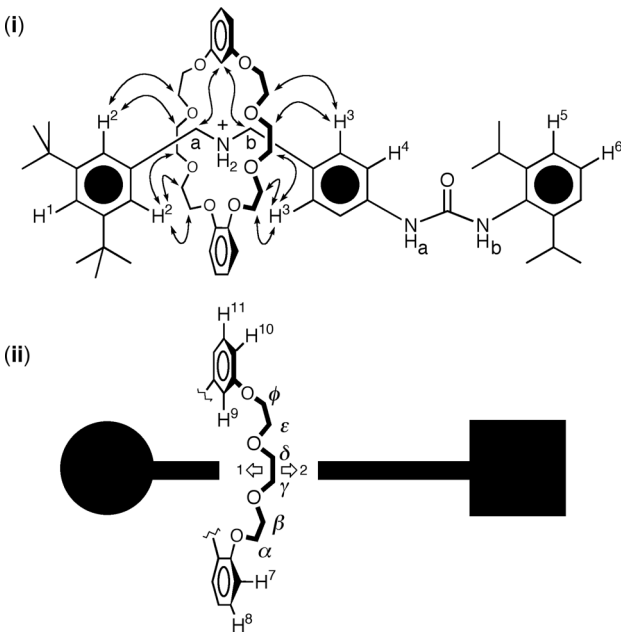

Figure 4.15. The structure of the [2]rotaxane **7**-$H{\cdot}O_2CCF_3$, showing the labeling scheme for the protons on both (**i**) the dumbbell and (**ii**) the crown ether components, used in describing its NMR spectroscopic parameters. The through-space correlations determined by T-ROESY measurements are also highlighted in (**i**) by double-headed arrows. The schematic representation (**ii**) highlights the unsymmetrical nature of the dumbbell. The protons (α^1, β^1, γ^1, δ^1, ε^1, ϕ^1) on one face of the BMP25C8 macrocycle are oriented toward the 3,5-di-*tert*-butylphenyl stopper, whereas those protons (α^2, β^2, γ^2, δ^2, ε^2, ϕ^2) on the opposite face of the macrocycle are directed toward the 2,6-diisopropylphenyl stopper.

dumbbell. Such an interaction is not possible in a DB24C8 system since there are no protons oriented toward the center of the macrocyclic cavity. Another interesting feature—also observed in the case of **1**-H·O_2CCF_3—is the inequivalence of the methyl groups that constitute the isopropyl moieties on one of the stoppers. This heterotopicity is manifest in the ^{13}C NMR spectrum, wherein two resonances are observed for the carbon atoms of the isopropyl methyl groups. On warming up an NMR sample of **7**-H·O_2CCF_3 dissolved in CD_3CN/CD_3SOCD_3 (3:1), the two resonances are observed (Figure 4.16) to coalesce[45] between 312 and 317 K, indicating that the inequivalence arises as a consequence of a slow bond rotation with an energy barrier in the range of $\Delta G^{\ddagger}$ = 15.0–15.2 kcal/mol. In order to determine the relative energetics of rotation about the groups attached to the 2,6-disubstituted stopper, a molecular mechanics investigation was undertaken. A Ramachandran-like plot (Figure 4.17) was constructed, whereby the torsion angles of the bonds from the phenyl group to the urea (defined by atoms C_o–C_i–N_u–H_u and referred to as θ) and to the isopropyl group (defined by atoms C_i–C_o–C_m–H_m and referred to as ϕ) were rotated by 360° in 10° increments from their initial angles of 90° and 0° respectively. All torsion angles were unconstrained except those being rotated. After construction of the model compound within the INPUT submode of MacroModel 5.5,[46] each set of torsion angles was varied sequentially, and the energy was minimized utilizing

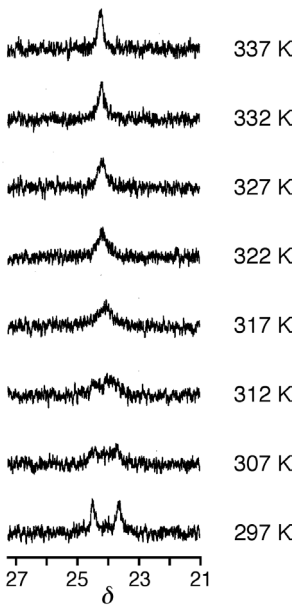

Figure 4.16. Partial ^{13}C NMR spectra (125 MHz, CD_3CN:CD_3SOCD_3 3:1), recorded at various temperatures, showing the coalescence of the signal arising from the carbon atom of the methyl groups that constitute the isopropyl groups.

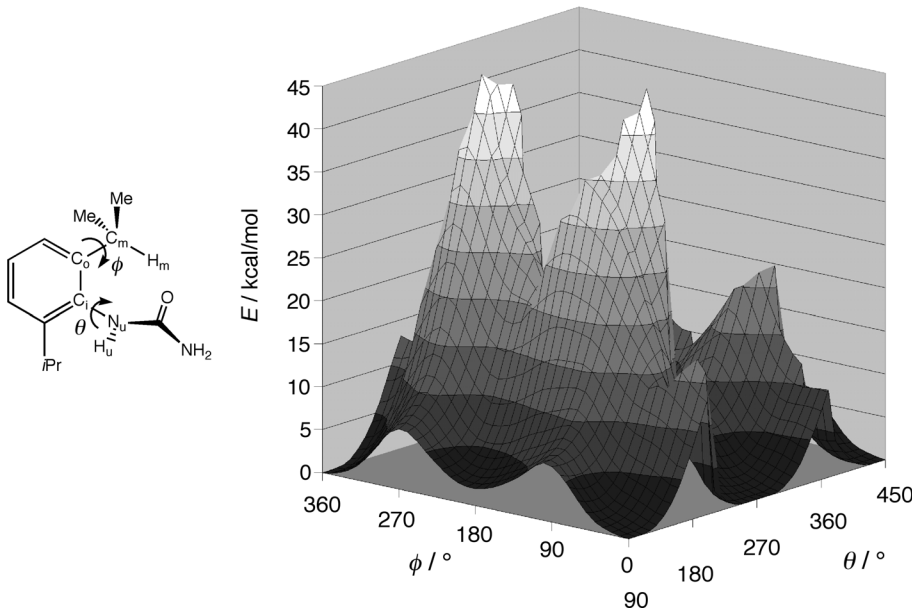

Figure 4.17. A Ramachandran-like plot depicting the energy profile of bond rotations associated with the 2,6-diisopropylphenyl stopper moiety.

MM3*—the MacroModel implementation of the MM3 force field[47] *via* the PRCG algorithm[48] using a maximum of 10000 iterations or until the final energy gradient fell below 0.05 kJ/Å. Solvation was considered through use of the GB/SA model[49] for chloroform. Each energy value was scaled relative to the lowest energy point found on the potential surface. The average height of the energy barrier corresponding to rotation of an isopropyl group is roughly 6.5 kcal/mol, whereas rotation of the N–Ar bond is significantly more hindered, showing an average energy barrier of 14 kcal/mol, a value which is in good agreement with that determined experimentally (15.0–15.2 kcal/mol). The energy profile is dominated by two large 'mountains', corresponding to the direct clashing of the ureido oxygen atom with the methyl groups of the isopropyl unit, and two smaller 'mountains' corresponding to steric interactions between the methyl groups and the ureido hydrogen atom. The rest of the profile is divided into two broad valleys running parallel to the axis denoted ϕ, reflecting relatively facile rotation of the isopropyl

group with respect to the phenyl ring. These valleys are lined with fairly high walls in the direction of θ, implying that rotation of the urea group is hindered more than rotation of the isopropyl units. The energy barrier to rotation about θ of 6.5 kcal/mol is easily surmountable at room temperature, whereas the 14 kcal/mol barrier will be significantly less readily overcome. It is reasonable to assume that the isopropyl groups are rotating rapidly about the ϕ bond, whereas rotation about the urea-phenyl bond is rapid on the NMR timescale only at elevated temperatures, as indicated by the coalescence between 312 and 317 K of the signal arising from the methyl carbon atom.

X-Ray Crystallography

Single crystals, suitable for X-ray crystallographic analysis, were obtained upon layering a CH_2Cl_2 solution of the [2]rotaxane **7**-H·O_2CCF_3 with hexanes. The structure (Figure 4.18) of the [2]rotaxane utilizing BMP25C8 (**8**) as the encircling macrocycle is very

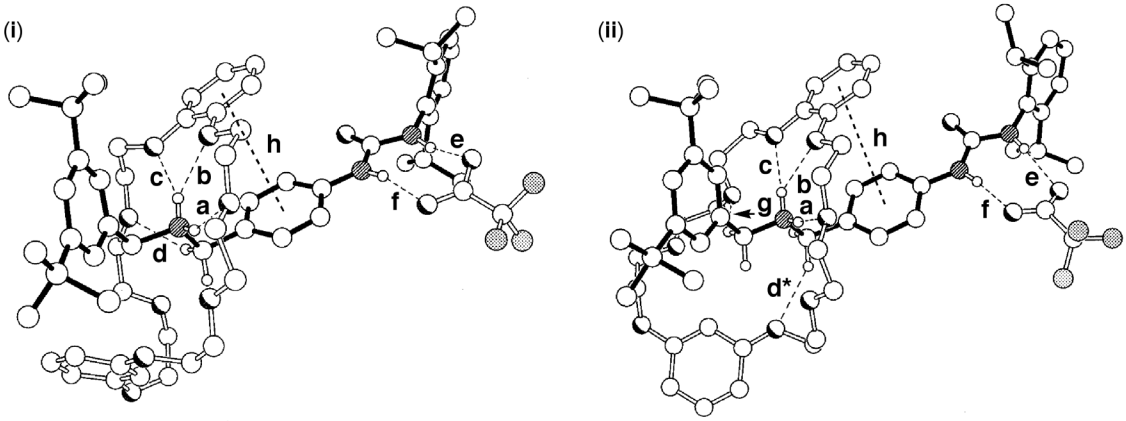

Figure 4.18. The molecular structures of the two crystallographically-independent [2]rotaxanes present in the crystals of **7**-H·O_2CCF_3. Hydrogen bonding distances and angles {[X···O], [H···O] distances (Å), [X–H···O] angles (°)}: for molecule (**i**); (**a**) 2.90, 2.07, 152; (**b**) 2.92, 2.17, 140; (**c**) 3.06, 2.26, 149; (**d**) 3.34, 2.48, 149; (**e**) 2.83, 1.95, 163; (**f**) 2.88, 2.00, 166; for molecule (**ii**); (**a**) 2.83, 1.94, 170; (**b**) 2.95, 2.34, 125; (**c**) 3.13, 2.26, 163; (**d***) 3.30, 2.43, 150; (**e**) 2.93, 2.04, 170; (**f**) 2.89, 2.00, 172; (**g**) 3.22, 2.42, 141. The centroid-centroid distances (**h**) for molecules (**i**) and (**ii**) are 4.22 and 4.29 Å, respectively.

similar to that of the DB24C8 analogue **1**-H·O_2CCF_3 in that the crystals contained two independent molecules in the asymmetric unit. In both of these molecules, the geometry of the cationic thread is very similar (Table 4.1) and differs only slightly from that observed in **1**-H·O_2CCF_3. The difference between the two crystallographically independent molecules of the [2]rotaxane **7**-H·O_2CCF_3 is in the relative orientations of the resorcinol ring systems with respect to the macrocycle as a whole. Stabilization of the [2]rotaxane is *via* a combination of N^+–H···O and C–H···O hydrogen bonds between the cation and the polyether macrocycle. As in **1**-H·O_2CCF_3, the urea component of the cation is hydrogen bonded to the trifluoroacetate anion. Also, in common with this [2]rotaxane, there is a similar apparent overlap between a catechol ring in the BMP25C8 macrocycle and the central *p*-toluidinyl ring of the cation. In both independent molecules, the two ring systems are inclined (by 19 and 24° in molecules **i** and **ii**, respectively) and the centroid-centroid separations are fairly long (4.22 and 4.29 Å in **i** and **ii**, respectively), thus minimizing any potential π–π interactions. It is interesting to note that the geometric relationship observed between these two ring systems in both independent molecules in **1**-H·O_2CCF_3 and **7**-H·O_2CCF_3 is probably a consequence of the adoption of a 'preferred' conformation for the cation and the ensuing sterically/hydrogen bonded enforced geometric relationship between the two components.

The only inter-[2]rotaxane feature of note is a C–H···π interaction between H-11 (as defined in Figure 4.15) of the resorcinol ring of molecule **i** and the 2,6-diisopropylphenyl ring of the cation in molecule **ii** (the H···π distance is 2.77 Å and the associated C–H···π angle is 154°).

4.3. A Thermodynamic Approach – Imine Formation

The following Section reports the use of the well-known reversible imine bond-forming reaction[50] to construct—using a stoppering approach (recall Figure 4.5)—a so-called dynamic [2]rotaxane, starting from a rod-like component terminated by aldehyde functions—specifically, the bis(4-formylbenzyl)ammonium ion (**9**-H·PF_6)—3,5-di-*t*-butylaniline (**12**), and a complementary ring component, namely DB24C8 (**5**).

4.3.1. A Dynamic [2]Rotaxane

The synthesis of the rod-like component (**9**-H·PF_6) is shown in Scheme 4.3. Reduction ($LiAlH_4$/THF) of the diester[51] **10** affords the diol **11** which is oxidized (PCC/CH_2Cl_2) to the dialdehyde **9**. Protonation (HCl/MeOH) of **9**, followed by counterion exchange (NH_4PF_6/H_2O), produces **9**-H·PF_6 in an overall yield of 37 %. As expected,[52] **9**-H·PF_6 forms a strong 1:1 complex with DB24C8 (**5**), both in solution and the 'gas phase', as evidenced by ^{1}H NMR spectroscopy and FAB mass spectrometry, respectively. Inspection of the ^{1}H NMR spectrum (400 MHz, CD_3CN, 20 mM, 300 K) of an equimolar mixture of these two components revealed (Figure 4.19) the presence of three sets of signals, corresponding to (i) the [2]pseudorotaxane [**5**·**9**-H]PF_6, (ii) uncomplexed **9**-H·PF_6, and (iii) free DB24C8 (**5**), indicating that these species are equilibrating slowly on the ^{1}H NMR timescale. As a consequence of this slow

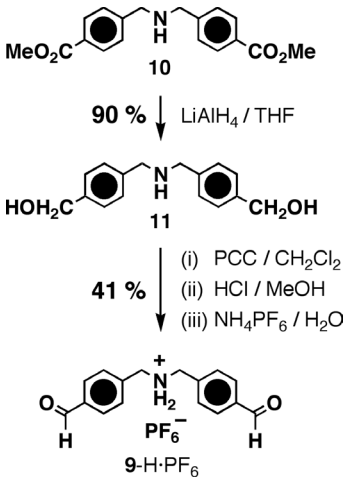

Scheme 4.3. Synthesis of the dialdehyde **9**-H·PF_6.

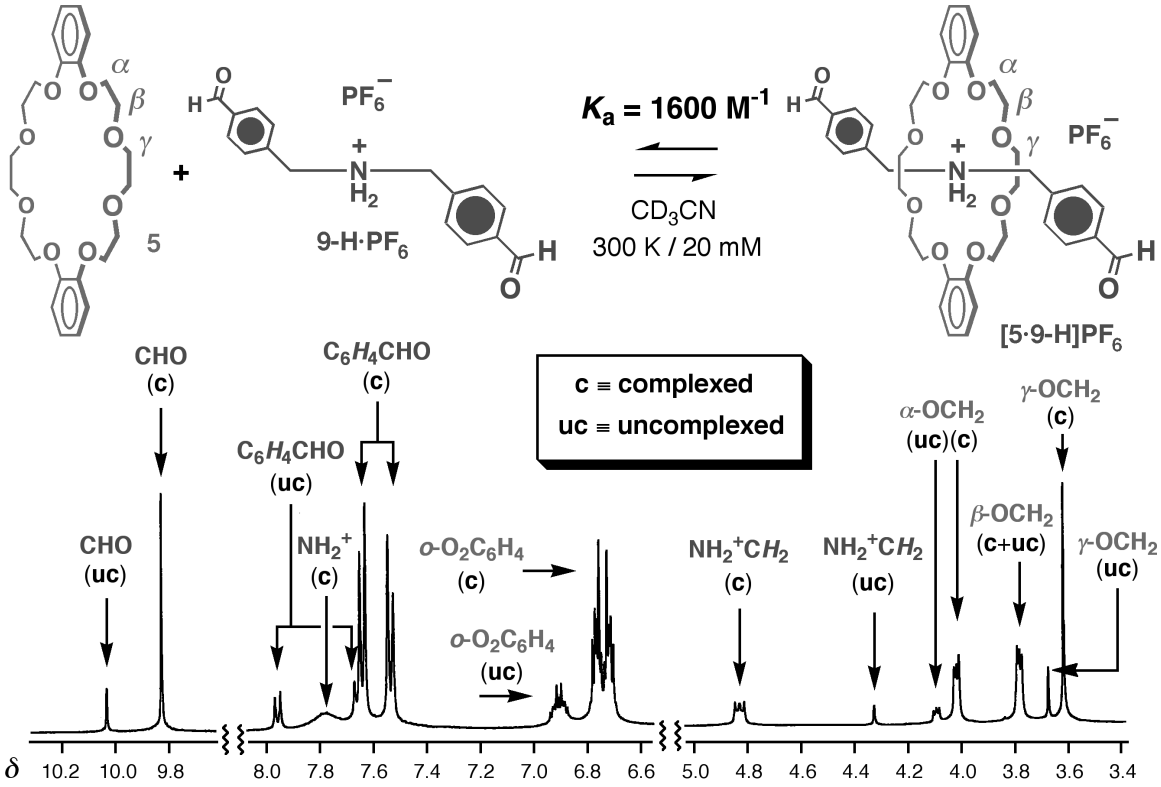

Figure 4.19. Signals for the resonances corresponding to (i) free crown ether **5** (ii) uncomplexed thread (**9**-H·PF_6) and (iii) the 1:1 pseudorotaxane complex ([**5**·**9**-H]PF_6) formed between the two individual components can be observed in the ^{1}H NMR spectrum. This phenomenon indicates that the free and complexed species are equilibrating slowly on the NMR timescale and therefore allows for the simple calculation of K_a by utilizing the so-called single-point method.

exchange, the association constant K_a was calculated[53] to be 1600 M^{-1} ($-\Delta G° = 4.4$ kcal mol^{-1}) by using the 'single-point method'.[54] Additionally, the base peak—which was observed at a value of *m/z* = 702—in the FAB mass spectrum of a 1:1 mixture of DB24C8 (**5**) and **9**-H·PF_6 corresponds to the [2]pseudorotaxane.

In the knowledge that the aromatic dialdehyde **9**-H·PF_6 complexes strongly in CD_3CN with DB24C8 (**5**), we examined its ability to form the dumbbell-shaped diimine **14**-H·PF_6, *via* the intermediacy of the monoimine **13**-H·PF_6, on addition of two equivalents of 3,5-di-*t*-butylaniline (**12**). The choice of this amine relates to the fact that (i) the 3,5-

di-*t*-butylphenyl group has been shown[55] to be sufficiently large to act as a stopper toward DB24C8 and (ii) the less basic aromatic amino group of the aniline will offer little competition for the proton attached to the much more basic aliphatic nitrogen atom present in **9**-H·PF_6. The reaction of **9**-H·PF_6 with 3,5-di-*t*-butylaniline (**12**) was monitored (Figure 4.20) by ^{1}H NMR spectroscopy. A 20 mM solution of **9**-H·PF_6 in

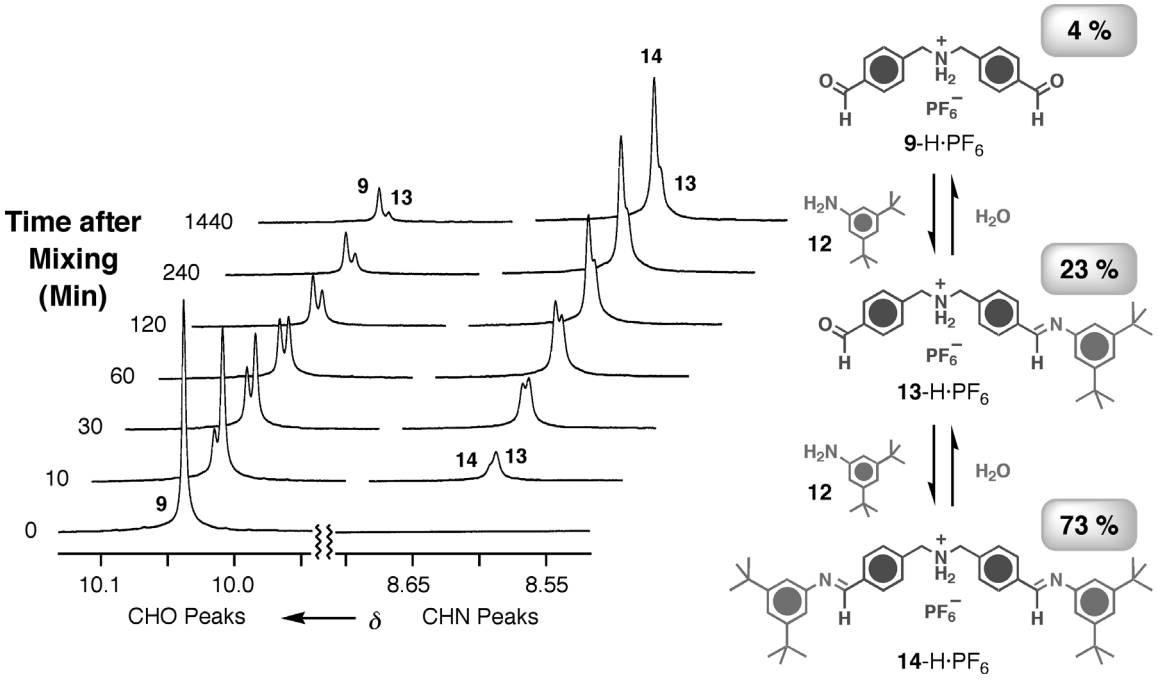

Figure 4.20. Left: Partial ^{1}H NMR spectra (400 MHz, CD_3CN, 300 K), recorded over time, of an initial mixture of dialdehyde **9**-H·PF_6 (20 mM) and 3,5-di-*tert*-butylaniline **12** (40 mM). Right: The dynamic equilibrium established in solution, and the corresponding percentages of each of the three species at equilibrium. The probe protons of, and the associated resonances for, the dialdehyde are labeled '**9**' (*i.e.*, corresponding to compound **9**-H·PF_6), those of the monoaldehyde (monoimine) '**13**', and those of the diimine dumbbell '**14**'.

CD_3CN was prepared and, after recording its ^{1}H NMR spectrum (t = 0 min), two equivalents of the aniline **12** were added and the ^{1}H NMR spectrum was recorded at appropriate time intervals. After 10 min, two singlets are observed for CHO protons: the more intense singlet corresponds to unreacted **9**-H·PF_6, while the smaller resonance arises

from **13**-H·PF_6. Two singlets, one each for **13**-H·PF_6 and **14**-H·PF_6, are also observed in the CHN region of the spectrum. During the course of the reaction, both CHO signals decrease in intensity, concomitant with the increasing intensity observed for the CHN peaks. Moreover, comparison of the spectra shows that, although initially the intermediate monoaldehyde/monoimine **13**-H·PF_6 is the major product, eventually, after 60 min, the diimine **14**-H·PF_6 starts to predominate. At equilibrium (1440 min = 1 day), integration of the CHO/CHN signals allows the product distribution, dialdehyde **9**-H·PF_6 (4 %), monoaldehyde/monoimine **13**-H·PF_6 (23 %) and diimine dumbbell **14**-H·PF_6 (73 %), to be calculated.[56] The implication of this equilibrium composition is that, on addition of one equivalent of DB24C8 (**5**) to the equilibrated mixture, no more than 27 % of it can encircle an NH_2^+ center, unless thermodynamic control is operating. The results are recorded in Figure 4.21. At t = 0 min, with no crown ether present, the spectrum is identical with the one recorded in Figure 4.20 at equilibrium (t = 1440 min). Upon

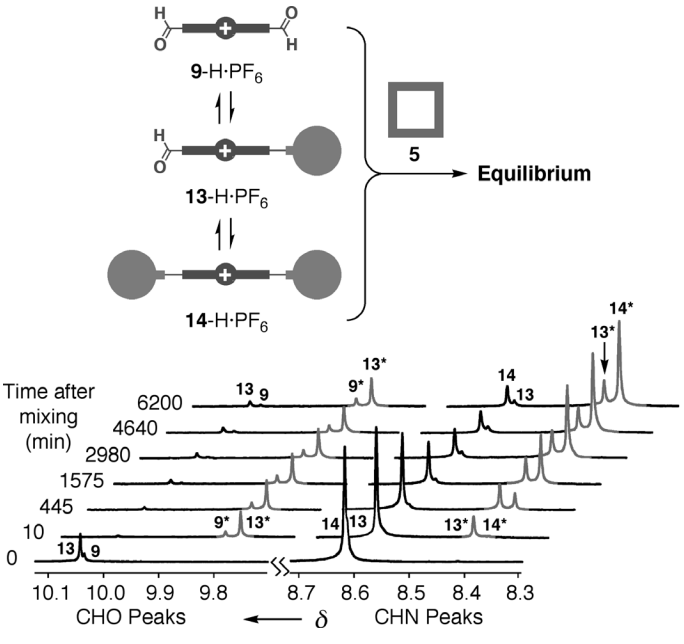

Figure 4.21. Top: A schematic representation of the dynamic process under spectroscopic investigation. Bottom: The partial ^{1}H NMR spectrum (400 MHz, CD_3CN, 300 K), recorded over time, of an initial mixture of **9**-H·PF_6 (20 mM), 3,5-di-*tert*-butyl-aniline **12** (40 mM), which was allowed to reach equilibrium (spectrum at t = 0 min) prior to the addition of DB24C8 (**5**) (20 mM). Peaks corresponding to species containing an NH_2^+ center not bound/occupied by a DB24C8 ring are colored black, while those which correspond to species that are bound/occupied are shaded grey and, furthermore, the numerical labels attached to these peaks are suffixed with an asterisk. The signals associated with the dialdehyde {**9**}, monoaldehyde {**13**} and diimine {**14**} probe protons are highlighted as described in Figure 4.20.

addition of DB24C8 (**5**), any species with an aldehyde group at either of its termini (*i.e.*, **9**-H·PF_6 and **13**-H·PF_6) is capable of threading through the crown ether's macrocyclic cavity, generating the corresponding [2]pseudorotaxane – *i.e.*, [**5**·**9**-H]PF_6 and [**5**·**13**-H]PF_6, respectively. This effect is seen immediately (t = 10 min), and subsequently, resonances corresponding to **9**-H·PF_6, **13**-H·PF_6, [**5**·**9**-H]PF_6, and [**5**·**13**-H]PF_6 remain substantially unchanged throughout the course of the experiment. By far the most predominant change observed in the spectra is the decrease in intensity of the peak at δ = 8.62 ppm (diimine dumbbell **14**-H·PF_6) and the corresponding growth of a new signal at δ = 8.37 ppm (diimine [2]rotaxane [**5**·**14**-H]PF_6). It is apparent, therefore, that, since the diimine dumbbell **14**-H·PF_6 *cannot* thread through the cavity of DB24C8 (**5**), the [2]rotaxane is being generated *via* a process in which consumption of **14**-H·PF_6 results in

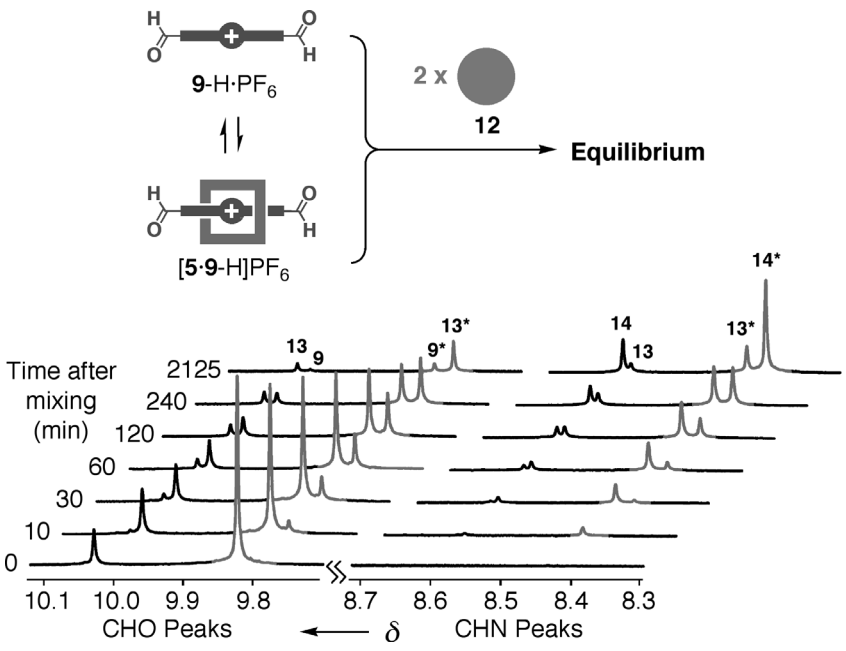

Figure 4.22. Top: A schematic representation of the dynamic process under spectroscopic investigation. Bottom: The partial ^{1}H NMR spectrum (400 MHz, CD_3CN, 300 K) recorded over time, of an initial mixture of **9**-H·PF_6 (20 mM), 3,5-di-*t*-butylaniline **12** (40 mM) and DB24C8 (**5**) (20 mM). Peaks are annotated in the same fashion as in Figure 4.21.

the formation of either monoaldehyde/monoimine (**13**-H·PF_6) or dialdehyde (**9**-H·PF_6) thread which, in turn, *can* pass through the cavity of the macrocyclic polyether and subsequently react to form the diimine [2]rotaxane [**5**·**14**-H]PF_6. At equilibrium (t = 6200 min = *ca*. 4.5 days), the product distribution is [**5**·**14**-H]PF_6 (47 %), **14**-H·PF_6 (16 %); [**5**·**13**-H]PF_6 (26 %), **13**-H·PF_6 (6 %); [**5**·**9**-H]PF_6 (4 %), **9**-H·PF_6 (1 %). The same equilibrium proportions of these six species can be reached—but much more quickly—in 2125 min (Figure 4.22) when DB24C8 (**5**) is present in the reaction mixture from the outset. This observation is yet another indication that thermodynamic control is operating in this system, as the same equilibrium composition is being reached, irrespective of the starting point of the reaction.

By utilizing the secondary ammonium ion/crown ether recognition motif to bring about the noncovalent synthesis of a [2]pseudorotaxane, in conjunction with reversible imine bond formation to stopper covalently the [2]pseudorotaxane and produce a dynamic

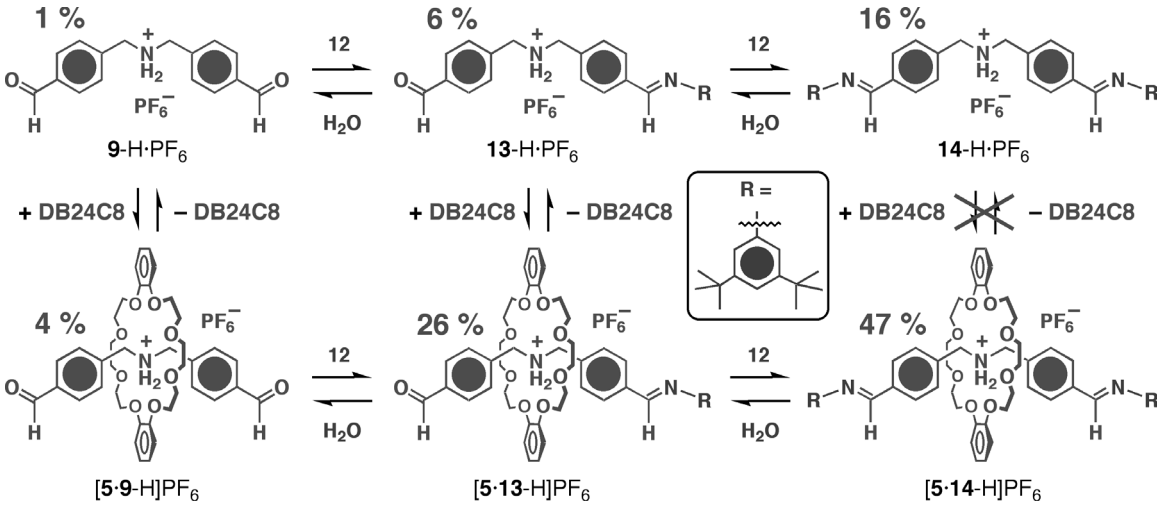

Scheme 4.4. The dynamic equilibrium established upon dissolution of a 1:2:1 ratio (20:40:20 mM) of **9**-H·PF_6, 3,5-di-*tert*-butylaniline (**12**) and DB24C8 (**5**) in CD_3CN.

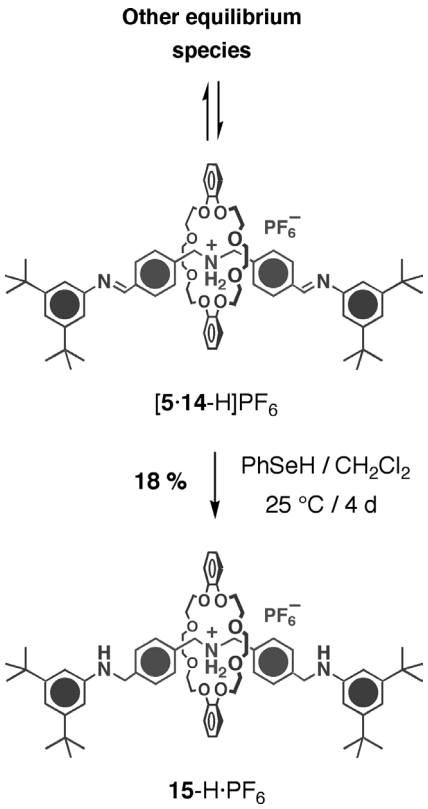

Scheme 4.5. 'Fixing' of the dynamic system upon reduction with PhSeH, thus affording the kinetically-stable [2]rotaxane **15**-H·PF_6.

[2]rotaxane, it has been demonstrated that thermodynamic control can be used in the construction of interlocked molecular compounds that are wholly organic in nature. A high degree of control of superstructure and structure can be envisaged in such 'slowly' equilibrating systems. For example, in Scheme 4.4, by judiciously altering solventpolarities,[38] the equilibria in the 'vertical' direction could be controlled, while removal of water from the reaction mixture should shift the equilibria in the 'horizontal' direction toward diimine formation. Thereafter, a 'fast' reduction of the imine bonds would give kinetically-stable products and, in so doing, 'fix' the [2]rotaxane. Indeed, initial investigations on the 'fixing' of this system—involving reduction of the imine functions—are encouraging. Treatment (Scheme 4.5) of an equilibrated mixture of **9**-H·PF_6, 3,5-di-*t*-butylaniline (**12**) and DB24C8 (**5**) in CH_2Cl_2 solution with PhSeH[57] affords the 'fixed' [2]rotaxane **15**-H·PF_6.

4.3.2. Future Outlook: Imine Exchange

The reversible nature of this particular system arises from the formation and hydrolysis of the imine bonds. Another strategy *via* which such structures can be assembled is that

of *imine exchange* (Figure 4.23). Isolation of the diimine dumbbell (**14**-H·PF_6) shown in Figure 4.23 would open up the possibility to do exchange reactions. For example, when the diimine dumbbell (**14**-H·PF_6) and DB24C8 (**5**) are mixed, no threading should occur, as the end-groups of the dumbbell are too large to pass through the cavity of this crown ether. However, the addition of a catalytic amount of a smaller aniline-containing molecule—such as *p*-toluidine (**16**)—should result in imine exchange, placing a small end-group on the dumbbell, which is now capable of threading through DB24C8's cavity. After formation of the [2]pseudorotaxane, another imine exchange reaction—with the

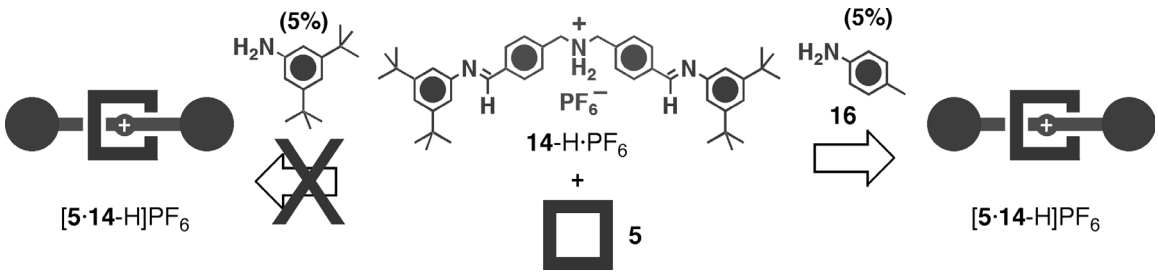

Figure 4.23. A schematic representation demonstrating the principle of thermodynamically-driven rotaxane synthesis *via* an imine exchange (rather than imine formation/hydrolysis) pathway.

larger aniline molecule—results in the formation of the [2]rotaxane. If only 5 % of the smaller amine is used, there can only be 5 % of end-groups, thus allowing for a high yield of [2]rotaxane. This result is obviously dependent upon the binding strength exhibited between the secondary ammonium center and the DB24C8 macrocycle, however, this interaction is relatively strong ($K_a \sim 10^4$ M^{-1}) in non-polar solvents such as CH_2Cl_2. Although not yet demonstrated in this system, imine exchange has been proven[58] to operate in the thermodynamic synthesis of rotaxanes based upon the dioxy-aryl/bipyridinium macrocycle recognition.

4.4. Conclusions

The *kinetic* synthesis of [2]rotaxanes—based upon the secondary ammonium ion/crown ether interaction—has been achieved by exploiting the reaction between amines and isocyanates to form ureas. Both DB24C8- and a BMP25C8-containing rotaxanes were formed, the latter of which represents the first example[59] of an interlocked structure incorporating this particular crown ether. The two ureido-[2]rotaxanes were characterized fully in the solution state—by using multiple 2D-NMR techniques—and the X-ray crystal structures of both compounds were also obtained. In contrast, imine formation/hydrolysis was exploited for the formation of a dynamic [2]rotaxane under *thermodynamic* control. Furthermore, it has been demonstrated that subsequent reduction (PhSeH) of the imine bonds present in this structure—a 'fixing' process—affords a kinetically-inert [2]rotaxane. Although kinetic approaches[60] have so far dominated the syntheses of interlocked molecular compounds with wholly organic constitutions, strategies involving thermodynamic control[61] are now set to challenge that domination. Such a sea-change in synthetic strategy is one that could lead to much more efficient routes, not only to rotaxanes[3] and catenanes,[2] but also to their macromolecular counterparts,[62] namely polyrotaxanes and polycatenanes. This goal may be achieved simply upon the reaction (Figure 4.24) of the secondary ammonium ion-containing

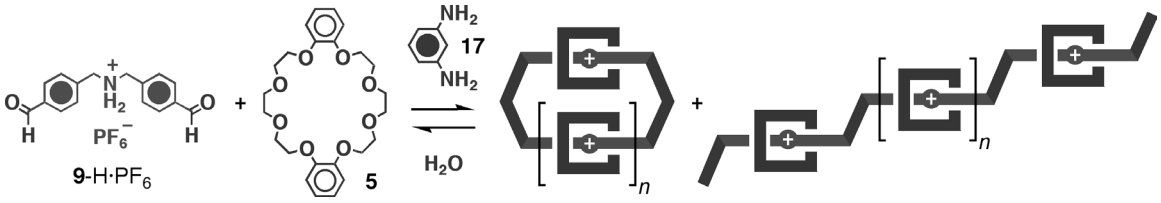

Figure 4.24. The reaction of the dialdehyde compound (**9**-H·PF_6) with a difunctional aniline (*e.g.*, *m*-phenylenediamine **17**) can yield two types of product. At lower concentrations, the formation of catenanes is anticipated, however, upon increasing the concentration, linear pseudopolyrotaxanes may be formed.

dialdehyde compound (**9**-H·PF_6) with dianilines (*e.g.*, **17**), rather than with bulky monoanilines, to yield, depending upon concentration, catenanes and/or pseudo-polyrotaxanes.

4.5. Experimental

General: Chemicals—including DB24C8 (**5**)—were purchased from Aldrich and used as received unless indicated otherwise. 3,5-Di-*t*-butylbenzaldehyde[40] (**2**), 4-azidobenzylamine[41] (**3**), and bis(4-methoxycarbonylbenzyl)amine[51] (**10**) were prepared according to literature procedures. For the synthesis of BMP25C8 (**8**), see Chapter 2 of this Thesis. Solvents were dried according to literature procedures.[63] Thin-layer chromatography was carried out using aluminium sheets precoated with silica gel 60F (Merck 5554). The plates were inspected by UV light and, if required, developed in I_2 vapor. Column chromatography was carried out using silica gel 60F (Merck 9385, 0.040–0.063 mm). Melting points were determined on an Electrothermal 9100 apparatus and are uncorrected. ^{1}H and ^{13}C NMR spectra were recorded on either a Bruker AC300 (300 and 75 MHz, respectively), Bruker ARX400 (400 and 100 MHz, respectively), or Bruker ARX500 (500 and 125 MHz, respectively) spectrometer, using residual solvent as the internal standard. All chemical shifts are quoted on the δ scale, and all coupling constants are expressed in Hertz (Hz). All 2D NMR experiments were recorded with 1K data points and 256 time increments in phase sensitive mode using TPPI, with the sample non-spinning. Double quantum filtered ^{1}H-^{1}H COSY experiments[64] were processed in a 1K x 1K matrix, and a forward linear prediction was performed in the F1 dimension. T-ROESY experiments[65] were performed with a spin lock mixing time of 300 ms, and processed in a 1K x 1K matrix with a forward linear prediction in the F1 dimension. All samples were degassed immediately before performing the T-ROESY experiments by sonicating the solution for approximately 30 min in an ultrasound bath. ^{1}H-^{13}C Correlation *via* heteronuclear zero and double quantum coherence (HMQC) experiments[66] were performed using BIRD sequence for presaturation of protons not attached to ^{13}C nuclei, and processed in a 1K x 1K matrix. Fast atom bombardment (FAB) mass spectra were obtained

using a ZAB-SE mass spectrometer, equipped with a krypton primary atom beam, utilizing a *m*-nitrobenzyl alcohol matrix. Cesium iodide or poly(ethylene glycol) were employed as reference compounds. Microanalyses were performed by either the University of North London Microanalytical Service (UK) or Quantitative Technologies, Inc (USA).

4-Aminobenzyl-3,5-di-*t*-butylbenzylamine Dihydrochloride (**4**-H_2·2Cl). 4-Azidobenzylamine[41] (**3**) (1.70 g, 11.5 mmol) and 3,5-di-*t*-butylbenzaldehyde[40] (**2**) (2.50 g, 11.5 mmol) were dissolved in C_6H_6 (100 mL), and the reaction mixture was heated under reflux over a 20 h period during which time the H_2O formed in the reaction was collected by means of a Dean-Stark trap. After allowing the reaction mixture to cool down to ambient temperature, MeOH (50 mL) was added to it. The subsequent portionwise addition of $NaBH_4$ (4.35 g, 115 mmol) was completed in 30 min, and the reaction mixture was left to stir for 4 d under ambient conditions. Hydrochloric acid (5N, 100 mL) was added and the solvents were removed *in vacuo*. The residue was partitioned between NaOH (2N, 250 mL) and CH_2Cl_2 (250 mL) and, upon separation, the aqueous portion was washed further with CH_2Cl_2 before the organic extracts were combined, dried ($MgSO_4$), and evaporated to dryness to afford a thick yellow oil. The oil was dissolved in CH_2Cl_2 (100 mL) and HCl gas was bubbled through this solution for 25 min. After stirring for a further 30 min, Et_2O (100 mL) was added and the solution became cloudy. It was reduced in volume to ~100 mL, before adding more Et_2O (100 mL). Filtration afforded the title compound as a pale yellow solid (3.85 g, 67 %); M.p. >200 °C (decomp.); ^{1}H NMR (400 MHz, CD_3SOCD_3): δ = 1.29 (s, 18H; $C(CH_3)_3$), 4.07–4.18 (m, 4H; CH_2–N–CH_2), 7.35 (d of an AA'BB', J = 8.4 Hz, 2H; ArH), 7.40 (m, 1H; ArH), 7.44 (m, 2H; ArH), 7.65 (d of an AA'BB', J = 8.4 Hz, 2H; ArH), 9.84 (br s, 2H; NH_2^+); ^{13}C NMR (100 MHz, CD_3SOCD_3): δ = 31.2 (CH_3), 34.6 ($C(CH_3)_3$), 49.3 and 50.4 (CH_2-N-CH_2), 122.2, 122.7, 124.4, 130.8, 131.1, 131.6, 133.7 and 150.6 (aromatic C); MS (FAB): *m/z* = 326 $[M–2Cl]^+$; $C_{22}H_{34}N_2Cl_2$·0.5H_2O (406.4): calcd C 65.01, H 8.68, N 6.89; found C 65.12, H 8.39, N 6.93.

General Procedure for Rotaxane Formation. The dichloride salt **4**-H_2·2Cl (*ca*. 1.0 g) was partitioned between CH_2Cl_2 (100 mL) and NaOH (100 mL). After stirring for 10 min,

the organic phase was collected, dried ($MgSO_4$), and evaporated to dryness. A portion of the residue (340 mg, 1.05 mmol) was dissolved in anhydrous CH_2Cl_2 and the crown ether (**5** or **8**) (1.41 g, 3.15 mmol) was added. Upon dissolution of the crown ether, trifluoroacetic acid (120 mg, 1.05 mmol) was added, and, after 5 min, 2,6-diisopropylphenyl isocyanate (**6**) (1.07 g, 5.25 mmol) was introduced into the reaction mixture which was stirred under ambient conditions for a further 5 d. The solvents were removed *in vacuo* and the residue subjected to chromatography (SiO_2: gradient elution with CH_2Cl_2/MeOH, 99:1 to 9:1) affording the pure rotaxane.

Data for the DB24C8-containing [2]rotaxane **1**-H·O_2CCF_3, isolated as an off-white powder (0.73 g, 64 %); M.p. 117–119 °C; ^{1}H NMR (400 MHz, CD_2Cl_2): δ = 1.19 (s, 30H; C(CH_3)$_3$ and CH(CH_3)$_2$), 3.32 (sept, J = 7.0 Hz, 2H; CH(CH$_3$)$_2$), 3.42–3.47 (m, 4H; H-γ^1), 3.52-3.58 (m, 4H; H-γ^2), 3.67–3.73 (m, 4H; H-β^1), 3.78–3.85 (m, 4H; H-β^2), 4.07–4.17 (m, 8H; H-α^1 and H-α^2), 4.45–4.49 (m, 2H; CH_2(b)), 4.68–4.71 (m, 2H; CH_2(a)), 6.79–6.85 (m, 4H; H-7), 6.88–6.95 (m, 4H; H-8), 7.10 (d of an AA'BB', J = 8.5 Hz, 2H; H-3), 7.14 (d, J = 7.5 Hz, 2H; H-5), 7.21–7.26 (m, 1H; H-6), 7.28 (d, J = 1.5 Hz, 2H; H-2), 7.35 (t, J = 1.5 Hz, 1H; H-1), 7.44 (d of an AA'BB', J = 8.5 Hz, 2H; H-4), 7.53 (br s, 2H; NH_2^+), 8.97 (s, 1H; NH(b)CO), 10.16 (s, 1H; NH(a)CO); ^{13}C NMR (100 MHz, $CDCl_3$): δ = 23.5 and 24.4 (CH(*C*H$_3$)$_2$), 28.6 (*C*H(CH$_3$)$_2$), 31.5 (C(*C*H$_3$)$_3$), 34.9 (*C*(CH$_3$)$_3$), 52.9 (CH_2(a)), 53.1 (CH_2(b)), 68.1 (C-α), 70.2 (C-β), 70.5 (C-γ), 112.8 (C-7), 118.4 (C-4), 122.0 (C-8), 122.4 (quaternary aromatic), 122.9 (C-5), 123.3 (C-1), 123.7 (C-2), 127.1 (C-6), 129.7 (C-3), 131.6, 133.2, 143.2, 147.4, 147.6 and 151.4 (quaternary aromatic), 155.7 (C=O); MS (FAB): m/z = 976 [M–O_2CCF_3]$^+$; $C_{61}H_{82}F_3N_3O_{11}$ (1090.3): calcd C 67.20, H 7.58, N 3.85; found C 66.68, H 7.55, N 3.58. X-Ray quality single crystals were obtained when a CH_2Cl_2 solution of **1**-H·O_2CCF_3 was layered with C_6H_{14}s. Crystal data for **1**-H·O_2CCF_3: $C_{59}H_{82}N_3O_9$·O_2CCF_3·1.3CH_2Cl_2, M = 1200.7, monoclinic, $P2_1/c$ (no. 14), a = 21.583(2), b = 39.539(5), c = 15.511(2) Å, β = 96.17(1)°, V = 13160(2) Å^3, Z = 8 (there are two crystallographically independent molecules in the asymmetric unit), D_c = 1.212 g cm^{-3}, μ($Cu_{K\alpha}$) = 16.6 cm^{-1}, F(000) = 5109, T = 203 K; clear rhombs, 0.83 × 0.33 × 0.30 mm, Siemens P4 rotating anode diffractometer, ω-scans, 16269 independent reflections. The

structure was solved by direct methods and all the major occupancy non-hydrogen atoms of the cations and anions were refined anisotropically (the non-hydrogen atoms of the solvent molecules isotropically) using full matrix least-squares based on F^2 to give R_1 = 0.129, wR_2 = 0.334 for 7255 independent observed reflections [$|F_o| > 4\sigma(|F_o|)$, $2\theta \leq 110°$] and 1482 parameters. All computations were carried out using the SHELXTL PC program system.[67] CCDC 138348.[68]

Data for the BMP25C8-containing [2]rotaxane **7**-H·O_2CCF_3, isolated as an off-white powder (0.41 g, 36 %); M.p. 102–105 °C; ^{1}H NMR (400 MHz, CD_2Cl_2): δ = 1.19 (br s, 12H; CH(CH_3)$_2$), 1.24 (s, 18H; C(CH_3)$_3$) 3.31 (sept, J = 7.0 Hz, 2H; CH(CH$_3$)$_2$), 3.35–3.70 (m, 12H; H-β, H-γ and H-δ) , 3.73–3.79 (m, 2H; H-ε^1), 3.80–3.86 (m, 2H; H-ε^2), 3.91–3.98 (m, 2H; H-α^1), 4.06–4.13 (m, 2H; H-α^2), 4.15–4.26 (m, 4H; H-ϕ), 4.27–4.32 (m, 2H; CH_2(b)), 4.39–4.45 (m, 2H; CH_2(a)), 6.58 (dd, J = 2.5 and 8.5 Hz, 2H; H-10), 6.64 (t, J = 2.5 Hz, 1H; H-9), 6.72–6.76 (m, 2H; H-7), 6.90–6.95 (m, 2H; H-8), 7.07 (d of an AA'BB', J = 8.5 Hz, 2H; H-3), 7.14 (d, J = 7.5 Hz, 2H; H-5), 7.21–7.27 (m, 2H; H-6 and H-11), 7.30 (d, J = 1.5 Hz, 2H; H-2), 7.43 (t, J = 1.5 Hz, 1H; H-1), 7.48 (d of an AA'BB', J = 8.5 Hz, 2H; H-4), 7.73 (br s, 2H; NH_2^+), 8.94 (s, 1H; NH(b)CO), 10.23 (s, 1H; NH(a)CO); ^{13}C NMR (100 MHz, $CDCl_3$): δ = 23.5 and 24.4 (CH(*C*H$_3$)$_2$), 28.6 (*C*H(CH$_3$)$_2$), 31.5 (C(*C*H$_3$)$_3$), 35.0 (*C*(CH$_3$)$_3$), 52.7 (CH_2(a)), 53.2 (CH_2(b)), 67.9 (C-ϕ), 68.1 (C-α), 69.7 (C-β), 70.4 (C-ε), 70.7 (C-δ), 71.1 (C-γ), 103.9 (C-9), 107.6 (C-10), 112.5 (C-7), 118.5 (C-4), 121.3 (quaternary aromatic), 122.3 (C-8), 122.9 (C-5), 123.8 (C-1 and C-2), 127.2 (C-6), 129.8 (quaternary aromatic), 130.6 (C-3), 131.0 (C-11), 133.1, 143.5, 146.5, 147.5 and 151.8 (quaternary aromatic), 155.6 (C=O), 159.7 (quaternary aromatic); MS (FAB): *m/z* = 976 [M–O_2CCF_3]$^+$; $C_{61}H_{82}F_3N_3O_{11}$ (1090.3): calcd C 67.20, H 7.58, N 3.85; found C 67.66, H 7.70, N 3.78. X-Ray quality single crystals were obtained when a CH_2Cl_2 solution of **7**-H·O_2CCF_3 was layered with C_6H_{14}s. Crystal data for **7**-H·O_2CCF_3: $C_{59}H_{82}N_3O_9$·CF_3CO_2·0.25CH_2Cl_2·0.25MeCN, M = 1121.8, triclinic, space group $P\bar{1}$ (no. 2), a = 14.966(2), b = 22.879(3), c = 22.915(2) Å, α = 64.64(1), β = 72.82(1), γ = 76.20(1)°, V = 6717(2) Å^3, Z = 4 (there are two crystallographically independent molecules in the asymmetric unit), ρ_c = 1.109 g cm^{-3}, μ($Cu_{K\alpha}$) = 8.41 cm^{-1}, F(000) = 2400, T = 193 K; clear rhombs, 1.00 x 0.37 x

0.13 mm, Siemens P4/RA diffractometer, graphite-monochromated $Cu_{K\alpha}$ radiation, ω-scans, 16840 independent reflections. The structure was solved by direct methods. In each of the independent molecules disorder was found in one of the polyether arms and in both of the *tert*-butyl groups; disorder was also present in one of the $CF_3CO_2^-$ anions. In each case this was resolved into two partial occupancy orientations with the non-hydrogen atoms of the major occupancy orientations being refined anisotropically (those of the minor occupancy orientations were refined isotropically). The remaining non-hydrogen atoms of the [2]rotaxanes and the anions were refined anisotropically, whilst those of the solvent molecules were refined isotropically. The N–H and C–H hydrogen atoms were placed in calculated positions, assigned isotropic thermal parameters, $U(H) = 1.2U_{eq}(C/N)$ [$U(H) = 1.5U_{eq}$(C-Me)], and allowed to ride on their parent atoms. Refinements were by full matrix least-squares based on F^2 to give $R_1 = 0.162$, $wR_2 = 0.420$ for 7798 independent observed reflections [$|F_o| > 4\sigma(|F_o|)$, $2\theta \leq 115°$] and 1548 parameters. All computations were carried out using the SHELXTL PC program system.[67] CCDC 138349.[68]

Bis(4-hydroxymethylbenzyl)amine (**11**). A solution of bis(4-methoxycarbonylbenzyl)-amine[51] (**10**) (10.6 g, 33.8 mmol) in dry THF (500 mL) was treated with $LiAlH_4$ (5.6 g, 148 mmol). The reaction mixture was heated under reflux for 20 h and subsequently quenched with an excess of 5N HCl. The THF solution was decanted and the residue partitioned between 2N NaOH (250 mL) and CH_2Cl_2 (250 mL). The combined organic extracts were washed with 2N NaOH, dried (Na_2SO_4) and the solvents removed *in vacuo* to afford **11** (7.8 g, 90 %) as a white solid; M.p. 84–85 °C; ^{1}H NMR (200 MHz, $CDCl_3$, 298 K): δ = 3.78 (s, 4H), 4.66 (s, 4H), 7.31 (s, 8H); ^{13}C NMR (75.5 MHz, $CDCl_3$, 293 K): δ = 52.9, 65.2, 127.3, 128.5, 139.7, 139.8; MS (FAB): *m/z* = 258 $[M+H]^+$; $C_{16}H_{19}NO_2$ (257.3): calcd C 74.68, H 7.44, N 5.44; found C 74.71, H 7.49, N 5.40.

Bis(4-formylbenzyl)ammonium Hexafluorophosphate (**9**-H·PF_6). A solution of **11** (2.17 g, 8.4 mmol) in dry CH_2Cl_2 (150 mL) was treated with PCC (5.45 g, 25.3 mmol) and stirred under ambient conditions for 1.5 h. The reaction mixture was filtered through Celite, which was subsequently washed with Et_2O (150 mL) and MeOH (100 mL). 12N HCl (100

mL) was added to the solution and washings prior to the solvents being removed *in vacuo*. The solid residue was partitioned between 2N NaOH (250 mL) and CH_2Cl_2 (250 mL) and the organic layer was washed exhaustively with more 2N NaOH until it was colorless. The oily residue, obtained upon removal of the solvent, was subjected to column chromatography (SiO_2: CH_2Cl_2/MeOH, 99:1). Treatment of the purified dialdehyde with an excess of methanolic HCl, followed by concentration under reduced pressure, gave a slurry, which was poured into Et_2O (500 mL). The solid was recovered by filtration and dissolved in hot H_2O, to which an excess of aqueous NH_4PF_6 was added, resulting in the precipitation of a white solid, which was washed (Et_2O), and subsequently dried to afford **9**-H·PF_6 (1.37 g, 41 %); M.p. 158–161 °C (decomp.); ^{1}H NMR (400 MHz, CD_3CN, 300 K): δ = 4.35 (s, 4H), 7.67 (d, J = 8 Hz, 4H), 7.97 (d, J = 8 Hz, 4H), 10.04 (s, 2H); ^{13}C NMR (100 MHz, CD_3CN, 300 K): δ = 52.3, 131.0, 132.0, 137.4, 138.4, 193.3; MS (FAB): m/z = 254 $[M–PF_6]^+$; $C_{16}H_{16}NO_2 \cdot H_2O$ (417.28): calcd C 46.05, H 4.35, N 3.36; found C 46.08, H 4.18, N 3.25.

Reduction of the Dynamic [2]Rotaxane. An excess of PhSeH (1.0 g, 6.4 mmol) was added to an equilibrated (*ca*. 3 d stirring under ambient conditions) mixture of **9**-H·PF_6 (0.25 g, 0.6 mmol), DB24C8 (**5**) (0.56 g, 1.3 mmol) and 3,5-di-*t*-butylaniline (**12**) in dry CH_2Cl_2 (10 mL). The reaction mixture was stirred for 4 d under ambient conditions, before being poured into Et_2O (500 mL). A white solid was recovered upon filtration and subjected to column chromatography (SiO_2: CH_2Cl_2, then CH_2Cl_2/MeOH, 99:1). Although fractions containing the 'fixed' [2]rotaxane as the major product were collected, DB24C8 (**5**) co-elutes from the column with this compound, accounting for ~10 % (by mass) of the isolated white solid, as determined by ^{1}H NMR spectroscopy. Based on the ^{1}H NMR spectrum, the yield for the conversion of **9**-H·PF_6 into **15**-H·PF_6 was calculated to be 18 %. Selected data for **15**-H·PF_6: ^{1}H NMR (400 MHz, CD_2Cl_2, 300 K): δ = 1.25 (s, 36H), 3.48 (s, 8H), 3.73–3.77 (m, 8H), 4.04–4.09 (m, 8H), 4.25 (s, 4H), 4.60–4.65 (m, 4H), 6.45 (d, J = 1.6 Hz, 4H), 6.75–6.80 (m, 6H), 6.88–6.94 (m, 4H), 7.22 (AA' of AA'BB' system, J = 8.0 Hz, 4H), 7.29 (BB' of AA'BB' system, J = 8.0 Hz, 4H), 7.57 (br s, 2H); ^{13}C NMR (100 MHz, CD_2Cl_2, 300 K): δ = 31.7, 35.2, 48.3, 52.9, 68.6, 70.8, 71.3, 108.1, 112.7, 113.2, 118.1, 122.1, 128.2, 129.9, 131.0, 142.1, 148.1, 152.3; MS (FAB): m/z = 1081 $[M–PF_6]^+$.

4.6. References and Notes

1. (a) Schill, G. *Catenanes, Rotaxanes and Knots*; Academic: New York, 1971. (b) Amabilino, D. B.; Stoddart, J. F. *Chem. Rev.* **1995**, *95*, 2725–2828. (c) Vögtle, F.; Dunnwald, T.; Schmidt, T. *Acc. Chem. Res.* **1996**, *29*, 451–460. (d) Breault, G. A.; Hunter, C. A.; Mayers, P. C. *Tetrahedron* **1999**, *55*, 5265–5293. (e) Hubin, T. J.; Kolchinski, A. G.; Vance, A. L.; Busch, D. H. *Adv. Supramol. Chem.* **1999**, *5*, 237–357. (f) *Molecular Catenanes, Rotaxanes and Knots*; Sauvage, J.-P., Dietrich-Buchecker, C., Eds.; VCH-Wiley: Weinheim, 1999.
2. (a) Dietrich-Buchecker, C. O.; Sauvage, J.-P.; Kintzinger, J.-P. *Tetrahedron Lett.* **1983**, *46*, 5095–5098. (b) Hunter, C. A. *J. Am. Chem. Soc.* **1992**, *114*, 5303–5311. (c) Johnston, A. G.; Leigh, D. A.; Pritchard, R. J.; Deegan, M. D. *Angew. Chem., Int. Ed. Engl.* **1995**, *34*, 1209–1212. (d) Nielsen, M. B.; Li, Z. T.; Becher, J. *J. Mater. Chem.* **1997**, *7*, 1175–1187. (e) Fujita, M. *Acc. Chem. Res.* **1999**, *32*, 53–61. (f) Andrievsky, A.; Ahuis, F.; Sessler, J. L.; Vögtle, F.; Gudat, D.; Moini, M. *J. Am. Chem. Soc.* **1998**, *120*, 9712–9713. (g) Amabilino, D. B.; Ashton, P. R.; Balzani, V.; Boyd, S. E.; Credi, A.; Lee, J.-Y.; Menzer, S.; Stoddart, J. F.; Venturi, M.; Williams, D. J. *J. Am. Chem. Soc.* **1998**, *120*, 4295–4307. (h) Roh, S. G.; Park, K. M.; Park, G. J.; Sakamoto, S.; Yamaguchi, K.; Kim, K. *Angew. Chem., Int. Ed.* **1999**, *38*, 638–641. (i) Hamilton, D. G.; Montalti, M.; Prodi, L.; Fontani, M.; Zanello, P.; Sanders, J. K. M. *Chem. Eur. J.* **2000**, *6*, 608–617.
3. For the first reported synthesis of a [2]rotaxane, see: (a) Harrison, I. T.; Harrison, S. *J. Am. Chem. Soc.* **1967**, *89*, 5723–5724. For a representative selection of rotaxanes synthesized during the last decade, see: (b) Kolchinski, A. G.; Busch, D. H.; Alcock, N. W. *J. Chem. Soc., Chem. Commun.* **1995**, 1289–1291. (c) Ashton, P. R.; Ballardini, R.; Balzani, V.; Belohradsky, M.; Gandolfi, M. T.; Philp, D.; Prodi, L.; Raymo, F. M.; Reddington, M. V.; Spencer, N.; Stoddart. J. F.; Venturi, M.; Williams, D. J. *J. Am. Chem. Soc.* **1996**, *118*, 4931–4951. (d) Leigh, D. A.; Murphy, A.; Smart, J. P.; Slawin, A. M. Z. *Angew. Chem., Int. Ed. Engl.* **1997**, *36*, 728–732. (e) Anderson, S.; Claridge, T. D. W.; Anderson, H. L. *Angew. Chem., Int. Ed. Engl.* **1997**, *36*, 1310–1313. (f) Loeb, S. J.; Wisner, J. A. *Chem. Commun.* **1998**, 2757–2758. (g) Solladie, N.; Chambron, J.-C.; Sauvage, J.-P. *J. Am. Chem. Soc.* **1999**, *121*, 3684–3692. (h) Seel, C.; Vögtle, F. *Chem. Eur. J.* **2000**, *6*, 21–24. (i) Baer, A. J.; Macartney, D. H. *Inorg. Chem.* **2000**, *39*, 1410–1417.
4. Some intriguing interlocked (and intertwined) structures are eluded to in a special issue of *New J. Chem.* (**1993**, *17*, 617–763) devoted solely to 'Topology in Molecular Chemistry'. Additionally, for recent strategies concerning the synthesis of novel interlocked molecules, see: Chang, T.; Heiss, A. M.; Cantrill, S. J.; Fyfe, M. C. T.; Pease, A. R.; Rowan, S. J.; Stoddart, J. F.; Williams, D. J. *Org. Lett.* **2000**, *2*, 2943–2946.

5. (a) Seeman, N. C. *Acc. Chem. Res.* **1997**, *30*, 357–363. (b) Mao, C.; Sun, W.; Seeman, N. C. *Nature* **1997**, *386*, 137–138. (c) Ibukuro, F.; Fujita, M.; Yamaguchi, K.; Sauvage, J.-P. *J. Am. Chem. Soc.* **1999**, *121*, 11014–11015. (d) Rowan, S. J.; Cantrill, S. J.; Stoddart, J. F.; White, A. J. P.; Williams, D. J. *Org. Lett.* **2000**, *2*, 759–762. (e) Reuter, C.; Mohry, A.; Sobanski, A.; Vögtle, F. *Chem. Eur. J.* **2000**, *6*, 1674–1682.

6. The chemical structure of a [2]rotaxane appeared on the front page of the New York Times on Friday, July 16, 1999, in an article entitled, "Tiniest Circuits Hold Prospect of Explosive Computer Speeds". For the original article, see: Collier, C. P.; Wong, E. W.; Belohradsky, M.; Raymo, F. M.; Stoddart, J. F.; Kuekes, P. J.; Williams, R. S.; Heath, J. R. *Science* **1999**, *285*, 391–394.

7. Gale, P. A. *Philos. Trans. R. Soc. London, Ser. A* **2000**, *358*, 431–453.

8. (a) Balzani, V.; Gómez-López, M.; Stoddart, J. F. *Acc. Chem. Res.* **1998**, *31*, 405–414. (b) Sauvage, J.-P. *Acc. Chem. Res.* **1998**, *31*, 611–619. (c) Drexler, K. E. *Trends Biotechnol.* **1999**, *17*, 5–7. (d) Mao, C. D.; Sun, W. Q.; Shen, Z. Y.; Seeman, N. C. *Nature* **1999**, *397*, 144–146. (e) Asfari, Z.; Vicens, J. *J. Incl. Phenom.* **2000**, *36*, 103–118. (f) Yurke, B.; Turberfield, A. J.; Mills, A. P.; Simmel, F. C.; Neumann, J. L. *Nature* **2000**, *406*, 605–608. (g) Shigekawa, H.; Miyake, K.; Sumaoka, J.; Harada, A.; Komiyama, M. *J. Am. Chem. Soc.* **2000**, 122, 5411–5412. (h) Balzani, V.; Credi, A.; Raymo, F. M.; Stoddart, J. F. *Angew. Chem., Int. Ed.* **2000**, *39*, 3348–3391.

9. The challenge of nanofabrication—and hence the creation of nanomachines—was laid down by the physicist Richard Feynman in a lecture entitled, "There's Plenty of Room at the Bottom", delivered on December 29th, 1959, at the annual meeting of the American Physical Society at the California Institute of Technology. See, (a) Feynman, R. P. *Eng. Sci.* **1960**, *23*, 22–36. (b) Feynman, R. P. *Sat. Rev.* **1960**, *43*, 45–47.

10. (a) Boyer, P. D. *Angew. Chem., Int. Ed.* **1998**, *37*, 2297–2307. (b) Berg, H. C. *Nature* **1998**, *394*, 324–325. (c) Davis, A. P. *Nature* **1999**, *401*, 120–121. (d) Kelly, T. R.; De Silva, H.; Silva, R. A. *Nature* **1999**, *401*, 150–152. (e) Koumura, N.; Zijlstra, R. W. J.; van Delden, R. A.; Harada, N.; Feringa, B. L. *Nature* **1999**, *401*, 152–155. (f) Boyer, P. D. *Nature* **1999**, *402*, 247–249. (g) Raehm, L.; Kern, J.-M.; Sauvage, J.-P. *Chem. Eur. J.* **1999**, *5*, 3310–3317. (h) Ward, M. D. *Chem. Ind.* **2000**, 22–26. (i) Kelly, T. R.; Silva, R. A.; De Silva, H.; Jasmin, S.; Zhao, Y. J. *J. Am. Chem. Soc.* **2000**, *122*, 6935–6949. (j) Bermudez, V.; Capron, N.; Gase, T.; Gatti, F. G.; Kajzar, F.; Leigh, D. A.; Zerbetto, F.; Zhang, S. W. *Nature* **2000**, *406*, 608–611.

11. (a) Bissell, R. A.; Cordova, E.; Kaifer, A. E.; Stoddart, J. F. *Nature* **1994**, *369*, 133–137. (b) Livoreil, A.; Sauvage, J.-P.; Amaroli, N.; Balzani, V.; Flamigni, L.; Ventura, B. *J. Am. Chem. Soc.* **1997**, *119*, 12114–12124. (c) Ward, M. D. *Chem. Ind.* **1997**, 640–645. (d) Ashton, P. R.; Ballardini, R.; Balzani, V.; Baxter, I.; Credi, A.; Fyfe, M. C. T.; Gandolfi, M. T.; Gómez-López, M.; Martínez-Díaz, M.-V.; Piersanti, A.; Spencer, N.; Stoddart, J. F.; Venturi, M.; White, A. J. P.; Williams, D. J. *J. Am. Chem. Soc.* **1998**, *120*, 11932–11942. (e) Armaroli, N.; Balzani, V.; Collin, J.-P.; Gavina, P.; Sauvage, J.-P.; Ventura, B. *J. Am. Chem. Soc.* **1999**, *121*, 4397–4408.

(f) Balzani, V.; Credi, A.; Mattersteig, G.; Matthews, O. A.; Raymo, F. M.; Stoddart, J. F.; Venturi, M.; White, A. J. P.; Williams, D. J. *J. Org. Chem.* **2000**, *65*, 1924–1936. (g) Ashton, P. R.; Ballardini, R.; Balzani, V.; Credi, A.; Dress, R.; Ishow, E.; Kleverlaan, C. J.; Kocian, O.; Preece, J. A.; Spencer, N.; Stoddart, J. F.; Venturi, M.; Wenger, S. *Chem. Eur. J.* **2000**, *6*, 3558–3574.

12. (a) Reed, M. A.; Zhou, C.; Muller, C. J.; Burgin, T. P.; Tour, J. M. *Science* **1997**, *278*, 252–254. (b) Heath, J. R.; Kuekes, P. J.; Snider, G. S.; Williams, R. S. *Science* **1998**, *280*, 1716–1721. (c) Chen, J.; Reed, M. A.; Rawlett, A. M.; Tour, J. M. *Science* **1999**, *286*, 1550–1552. (d) Heath, J. R. *Pure Appl. Chem.* **2000**, *72*, 11–20. (e) Reed, M. A.; Tour, J. M. *Sci. Am.* **2000**, *282*, 86–93. (f) Ratner, M. *Nature* **2000**, *404*, 137–138. (g) Ball, P. *Nature* **2000**, *406*, 118–120. (h) Wong, E. W.; Collier, C. P.; Belohradsky, M.; Raymo, F. M.; Stoddart, J. F.; Heath, J. R. *J. Am. Chem. Soc.* **2000**, *122*, 5831–5840. (i) Rueckes, T.; Kim, K.; Joselevich, E.; Tseng, G. Y.; Cheung, C. L.; Lieber, C. M. *Science* **2000**, *289*, 94–97. (j) Collier, C. P.; Mattersteig, G.; Wong, E. W.; Luo, Y.; Beverly, K.; Sampaio, J.; Raymo, F. M.; Stoddart, J. F.; Heath, J. R. *Science* **2000**, *289*, 1172–1175.
13. Wasserman, E. *J. Am. Chem. Soc.* **1960**, *82*, 4433–4434.
14. (a) Whitesides, G. M.; Mathias, J. P.; Seto, C. T. *Science* **1991**, *154*, 1312–1319. (b) Philp, D.; Stoddart, J. F. *Angew. Chem., Int. Ed. Engl.* **1996**, *35*, 1154–1196. (c) Sijbesma, R. P.; Meijer, E. W. *Curr. Opin. Colloid Interface Sci.* **1999**, *4*, 24–32.
15. Schill, G.; Lüttringhaus, A. *Angew. Chem., Int. Ed. Engl.* **1964**, *3*, 546–547.
16. (a) Lehn, J.-M. *Supramolecular Chemistry*; VCH: Weinheim, 1995. (b) *Comprehensive Supramolecular Chemistry,* (11 Vols); Atwood, J. L., Davies, J. E. D., MacNicol, D. D., Vögtle, F., Eds.; Pergamon: Oxford, 1996.
17. A complex in which an acyclic component is threaded through a cyclic one is reminiscent of a rotaxane lacking bulky end-groups and is thus termed a *pseudorotaxane*.
18. For recent examples, see: (a) Hansen, J. G.; Feeder, N.; Hamilton, D. G.; Gunter, M. J.; Becher, J.; Sanders, J. K. M. *Org. Lett.* **2000**, *2*, 449–452. (b) Raehm, L.; Hamann, C.; Kern, J.-M.; Sauvage, J.-P. *Org. Lett.* **2000**, *2*, 1991–1994; (c) Safarowsky, O.; Vogel, E.; Vögtle, F. *Eur. J. Org. Chem.* **2000**, 499–505. (d) Cabezon, B.; Cao, J.; Raymo, F. M.; Stoddart, J. F.; White, A. J. P.; Williams, D. J. *Chem. Eur. J.* **2000**, *6*, 2262–2273.
19. For recent examples, see: (a) Reuter, C.; Vögtle, F. *Org. Lett.* **2000**, *2*, 593–595. (b) Skinner, P. J.; Blair, S.; Kataky, R.; Parker, D. *New J. Chem.* **2000**, *24*, 265–268. (c) Kawaguchi, Y.; Harada, A. *Org. Lett.* **2000**, *2*, 1353–1356. (d) Loeb, S. J.; Wisner, J. A. *Chem. Commun.* **2000**, 845–846. (e) Buston, J. E. H.; Young, J. R.; Anderson, H. L. *Chem. Commun.* **2000**, 905–906. (f) Tachibana, Y.; Kihara, N.; Ohga, Y.; Takata, T. *Chem. Lett.* **2000**, 806–807.
20. For examples, see: (a) Philp, D.; Stoddart, J. F. *Synlett* **1991**, 445–458. (b) Li, Z.-T.; Stein, P. C.; Becher, J.; Jensen, D.; Moerk, P.; Svenstrup, N. *Chem. Eur. J.* **1996**, *2*, 624–633. (c) Leigh, D. A.; Murphy, A.; Smart, J. P.; Slawin, A. M. Z. *Angew. Chem., Int. Ed. Engl.* **1997**, *36*, 728–732.

(d) Ballardini, R.; Balzani, V.; Dehaen, W.; Dell'Erba, A. E.; Raymo, F. M.; Stoddart, J. F.; Venturi, M. *Eur. J. Org. Chem.* **2000**, 591–602.

21. (a) Ashton, P. R.; Belohradsky, M.; Philp, D.; Stoddart, J. F. *J. Chem. Soc., Chem. Commun.* **1993**, 1269–1274. (b) Macartney, D. H. *J. Chem. Soc., Perkin Trans. 2* **1996**, 2775–2778. (c) Raymo, F. M.; Stoddart, J. F. *Pure Appl. Chem.* **1997**, *69*, 1987–1997. (d) Heim, C.; Affeld, A.; Nieger, M.; Vögtle, F. *Helv. Chim. Acta* **1999**, *82*, 746–759. (e) Fyfe, M. C. T.; Raymo, F. M.; Stoddart, J. F. In *Stimulating Concepts on Chemistry*; Shibasaki, M., Stoddart, J. F., Vögtle, F., Eds.; VCH-Wiley: Weinheim, 2000, pp. 211–220.
22. The *slippage* approach was the last to be developed for template-directed syntheses of 'rotaxanes'. However, for early reports of statistical *slippage* syntheses, see: (a) Harrison, I. T. *J. Chem. Soc., Chem. Commun.* **1972**, 231–232. (b) Schill, G.; Beckmann, W.; Schweikert, N.; Fritz, H. *Chem. Ber.* **1986**, *119*, 2647–2655.
23. Raymo, F. M.; Houk, K. N.; Stoddart, J. F. *J. Am. Chem. Soc.* **1998**, *120*, 9318–9322.
24. (a) Asakawa, M.; Ashton, P. R.; Ballardini, R.; Balzani, V.; Belohradsky, M.; Gandolfi, M. T.; Kocian, O.; Prodi, L.; Raymo, F. M.; Stoddart, J. F.; Venturi, M. *J. Am. Chem. Soc.* **1997**, *119*, 302–310. (b) Handel, M.; Plevoets, M.; Gestermann, S.; Vögtle, F. *Angew. Chem., Int. Ed. Engl.* **1997**, *36*, 1199–1201. (c) Ashton, P. R.; Fyfe, M. C. T.; Schiavo, C.; Stoddart, J. F.; White, A. J. P.; Williams, D. J. *Tetrahedron Lett.* **1998**, *39*, 5455–5458.
25. Ashton, P. R.; Baxter, I.; Fyfe, M. C. T.; Raymo, F. M.; Spencer, N.; Stoddart, J. F.; White, A. J. P.; Williams, D. J. *J. Am. Chem. Soc.* **1998**, *120*, 2297–2307.
26. Leigh, D. A.; Wilson, A. J.; Kidd, T. J. *Book of Abstracts (Part 2), 218th ACS National Meeting*, 1999, ORGN 0243.
27. Fyfe, M. C. T.; Stoddart, J. F. *Acc. Chem. Res.* **1997**, *30*, 393–401.
28. For mention of the application of reversible covalent chemistry to the synthesis of receptors—capable of recognition and catalysis—utilizing a selection approach, see: (a) Brady, P. A.; Sanders, J. K. M. *Chem. Soc. Rev.* **1997**, *26*, 327–336. (b) Rowan, S. J.; Sanders, J. K. M. *Curr. Opin. Chem. Biol.* **1997**, *1*, 483–490. (c) Sanders, J. K. M. *Chem. Eur. J.* **1998**, *4*, 1378–1383. For a discussion on the *noncovalent synthesis* of synthetic receptors in a combinatorial fashion, see: (d) Timmerman, P.; Reinhoudt, D. N. *Adv. Mater.* **1999**, *11*, 71–74.
29. (a) Fujita, M.; Ibukuro, F.; Hagihara, H.; Ogura, K. *Nature* **1994**, 367, 720–723. (b) Try, A. C.; Harding, M. M.; Hamilton, D. G.; Sanders, J. K. M. *Chem. Commun.* **1998**, 723–724. In more recent times, reversible metal-ligand interactions have also been exploited for the syntheses of rotaxanes; for stoppering approaches, see: (c) Lyon, A. P.; Macartney, D. H. *Inorg. Chem.* **1997**, *36*, 729–736. (d) Baer, A. J.; Macartney, D. H. *Inorg. Chem.* **2000**, *39*, 1410–1417. (e) Chichak, K.; Walsh, M. C.; Branda, N. R. *Chem. Commun.* **2000**, 847–848. For a clipping approach, see: (f) Jeong, K.-S.; Choi, J. S.; Chang, S.-Y.; Chang, H.-Y. *Angew. Chem., Int. Ed.* **2000**, *39*, 1692–1695.

30. For an example of a [2]catenane synthesis—employing ring opening and ring closing metathesis (RORCM)—operating under thermodynamic control, see: (a) Kidd, T. J.; Leigh, D. A.; Wilson, A. J. *J. Am. Chem. Soc*. **1999**, *121*, 1599–1600. An earlier report of a [2]catenane synthesis using RORCM [(b) Hamilton, D. G.; Feeder, N.; Teat, S. J.; Sanders, J. K. M. *New J. Chem*. **1998**, 1019–1021] describes a system which does not operate strictly under thermodynamic control, as a consequence of slow reaction kinetics and solubility limitations. For an example of [2]catenane synthesis utilizing ring closing metathesis (RCM) see: (c) Mohr, B.; Weck, M.; Sauvage, J.-P.; Grubbs, R. H. *Angew. Chem., Int. Ed. Engl*. **1997**, *36*, 1308–1310.

31. For an example used in the synthesis of natural products, see: (a) Nadin, A.; Nicolaou, K. C. *Angew. Chem., Int. Ed. Engl*. **1996**, *35*, 1622–1656. For comments on how ketalization under thermodynamic control can be exploited in the resolution of racemates, see: (b) Davis, A. P. *Angew. Chem., Int. Ed. Engl*. **1997**, *36*, 591–594.

32. (a) Rowan, S. J.; Sanders, J. K. M. *Chem. Commun*. **1997**, 1407–1408. (b) Brady, P. A.; Sanders, J. K. M. *J. Chem. Soc., Perkin Trans. 1* **1997**, 3237–3253. (c) Rowan, S. J.; Sanders, J. K. M. *J. Org. Chem*. **1998**, *63*, 1536–1546. More recently, reversible palladium-catalyzed allyl transesterification has been employed in the synthesis of porphyrin-containing macrocycles, see: (d) Kaiser, G.; Sanders, J. K. M. *Chem. Commun*. **2000**, 1763–1764.

33. (a) Hioki, H.; Still, W. C. *J. Org. Chem*. **1998**, *63*, 904–905. (b) Tam-Chang, S.-W.; Stehouwer, J. S.; Hao, J. *J. Org. Chem*. **1999**, *64*, 334–335. (c) Otto, S.; Furlan, R. L. E.; Sanders, J. K. M. *J. Am. Chem. Soc*. **2000**, *122*, 12063–12064.

34. (a) Cousins, G. R. L.; Poulsen, S.-A.; Sanders, J. K. M. *Chem. Commun*. **1999**, 1575–1576. (b) Furlan, R. L. E.; Cousins, G. R. L.; Sanders, J. K. M. *Chem. Commun*. **2000**, 1761–1762.

35. Comina, P. J.; Philp, D.; Kariuki, B. M.; Harris, K. D. M. *Chem. Commun*. **1999**, 2279–2280.

36. Polyakov, V. A.; Nelen, M. I.; Nazarpack-Kandlousy, N.; Ryabov, A. D.; Eliseev, A. V. *J. Phys. Org. Chem*. **1999**, *12*, 357–363.

37. See, for example, how increasing the temperature of a solution containing a secondary ammonium ion/crown ether based self-complementary daisy chain monomer results (Chapter 3 of this Thesis) in the deaggregation of complexed superstructures.

38. Ashton, P. R.; Chrystal, E. J. T.; Glink, P. T.; Menzer, S.; Schiavo, C.; Spencer, N.; Stoddart, J. F.; Tasker, P. A.; White, A. J. P.; Williams, D. J. *Chem. Eur. J.* **1996**, *2*, 709–728.

39. In this case, the threaded 1:1 aggregate formed between the ring and rod components is termed a *semirotaxane* (for an early usage of this term, see: Born, M.; Ritter, H. *Makromol. Chem., Rapid Commun.* **1991**, *12*, 471–476.), rather than a *pseudorotaxane*, as one end of the rod-shaped molecule already possesses a bulky stopper group.

40. Newman, M. S.; Lee, L. F. *J. Org. Chem.* **1972**, *37*, 4468–4469.

41. McFadden, H. G.; Phillips, J. N. *Z. Naturforsch., C: Biosci.* **1990**, *45*, 196–206.

42. The protons of the $R_2NH_2^+$ center are far more acidic than those of the urea moiety (pK_as ~10 and >20, respectively), thus bestowing upon them a much greater capacity for hydrogen bonding.

Additionally, inspection of CPK space-filling molecular models reveals that insertion of the urea portion of the dumbbell into the cavity of the DB24C8 ring is not favored sterically as a consequence of the proximal 2,6-diisopropylphenyl group. Also, this geometry would result in an unfavorable electrostatic interaction between the carbonyl oxygen atom on the urea group and the ethereal oxygen atoms lining the perimeter of the macrocyclic cavity. Indeed, a brief Monte Carlo conformational search within MacroModel (1000 steps, all variable torsions considered, Amber* force field, GB/SA $CHCl_3$, extended nonbonded cutoffs of 4, 8, and 20 Å for van der Waals, hydrogen bonding and electrostatic interactions, respectively) of the complexes formed between 2,6-diisopropylcarbanilide and DB24C8 furnished a global minimum conformation in which the ureido proton closest to the diisopropylphenyl unit is sterically prevented from participating in hydrogen bonding interactions by virtue of its proximity to the two isopropyl moieties. The structure corresponding to the global minimum involves a lone hydrogen bond emanating from the sterically unhindered ureido proton to an ethereal oxygen atom of the crown ether, which is encircling the carbanilide derivative with a pseudorotaxane geometry. This phenomenon contrasts with the results of a similar experiment performed employing carbanilide (*N*,*N*-diphenylurea) as the thread compound, in which the global minimum structure involves the formation of hydrogen bonds from both ureido protons to one of the ethereal oxygen atoms. The carbonyl oxygen atom of the urea group constitutes an unfavorable electrostatic interaction, which repels the crown ether. Thus, in this case, the complete superstructure involves the crown ether interacting attractively with one side of the urea moiety, and repulsively with the other side. These results support the empirical hypothesis—deduced from some observations made on CPK space-filling molecular models and a consideration of the relative pK_a values—that the crown ether prefers to reside around the dialkylammonium center, rather than around the urea moiety.

43. Unfortunately, the resonances arising from α^1 and α^2 are isochronous. Cross-peaks between this multiplet and the signals corresponding to both H-2 and H-3 are observed. As a consequence of this overlap, it is impossible to deduce that the H-2 resonance *only* gives a cross-peak with the α^1 resonance, and the H-3 resonance *only* gives a cross-peak with the α^2 resonance. Based upon the patterns observed for the β and γ protons, however, it is not unreasonable to suppose, by analogy, that selective through-space interactions also occur for the α protons.

44. Although BMP25C8 does not bind secondary ammonium ions as strongly as DB24C8 (see Chapter 2 of this Thesis for an extended discussion), it still *does* bind them. Consequently, as no rotaxanes incorporating this crown ether had been reported previously, the ability to form a [2]rotaxane, using this crown ether, was investigated.

45. The poor signal-to-noise ratio obtained when recording these ^{13}C NMR spectra preclude the calculation of *accurate* thermodynamic and kinetic parameters for this dynamic process. However, assuming that the coalescence of the two signals—corresponding to the *i*Pr groups—does occur in the range 312–317 K, estimates for the kinetic and thermodynamic parameters for this process can be obtained as described in Sutherland, I. O. *Annu. Rep. NMR Spectrosc.* **1971**, *4*, 71–235. The rate

constant for this bond rotation (k_c) at the coalescence temperature (T_c) was calculated by employing the approximate expression $k_c = \pi(\Delta\nu)/(2)^{1/2}$, where $\Delta\nu$ is the limiting frequency difference (96 Hz) between the coalescing peaks. The relationship $\Delta G_c^{\ddagger} = -RT_c\ln(k_c h/k_B T_c)$—where R, h and k_B correspond, respectively, to the gas, Planck and Boltzmann constants—was used to determine the free activation barriers ($\Delta G_c^{\ddagger}$) of this bond rotation process at 312 and 317 K (T_c 'range'), thus giving the range 15.0–15.2 kcal/mol.

46. Mohamadi, F.; Richards, N. G. J.; Guida, W. C.; Liskamp, R.; Lipton, M.; Caulfield, C.; Chang, G.; Hendrickson, T.; Still, W. C. *J. Comput. Chem.* **1990**, *11*, 440–467.
47. Allinger, N. L.; Yuh, Y. H.; Lii, J. H. *J. Am. Chem. Soc.* **1989**, *111*, 8551–8566.
48. Polak, E.; Ribière, G. *Rev. Fr. Informat. Rech. Oper.* **1969**, *16*, 35–43.
49. Still, W. C.; Tempczyk, A.; Hawley, R. C.; Hendrickson, T. *J. Am. Chem. Soc.* **1990**, *112*, 6127–6129.
50. For a review of reactions of carbonyl compounds leading to the formation of carbon-nitrogen double bonds, see: Dayagi, S.; Degani, Y. in *The Chemistry of the Carbon-Nitrogen Double Bond*; Ed.: Patai, S.; Interscience, **1970**, pp. 64–83. For an example of how the reversible nature of imine bond formation can be exploited in conjunction with molecular recognition to alter the product selectivity in a 'virtual' combinatorial library, see: Huc, I.; Lehn, J.-M. *Proc. Natl. Acad. Sci. USA* **1997**, *94*, 2106–2110.
51. Ashton, P. R.; Glink, P. T.; Stoddart, J. F.; Tasker, P. A.; White, A J. P.; Williams, D. J. *Chem. Eur. J.* **1996**, *2*, 729–736.
52. Ashton, P. R.; Campbell, P. J.; Chrystal, E. J. T.; Glink, P. T.; Menzer, S.; Philp, D.; Spencer, N.; Stoddart, J. F.; Tasker, P. A.; Williams, D. J. *Angew. Chem., Int. Ed. Engl.* **1995**, *34*, 1865–1869.
53. The K_a value of 1600 M^{-1} is much greater than that observed in CD_3CN for the parent, unsubstituted dibenzylammonium hexafluorophosphate, which has been shown [Ashton, P. R.; Bartsch, R. A.; Cantrill, S. J.; Hanes, Jr., R. E.; Hickingbottom, S. K.; Lowe, J. N.; Preece, J. A.; Stoddart, J. F.; Talanov, V. S.; Wang, Z.-H. *Tetrahedron Lett*. **1999**, *40*, 3661–3664] to bind DB24C8 (**5**) with a K_a value of 320 M^{-1}. This observation is consistent with the decreased electron densities in the aromatic rings as a consequence of the electron withdrawing nature of the CHO group, which in turn is expected to increase the relative acidities of the cation's CH_2 and NH_2^+ protons, thus enhancing the binding capability of the thread-like molecule within the crown ether's cavity. For a discussion concerning the effect of electron donating/withdrawing group substitution of the phenyl rings associated with the dibenzylammonium ion, see: Ashton, P. R.; Fyfe, M. C. T.; Hickingbottom, S. K.; Stoddart, J. F.; White, A. J. P.; Williams, D. J. *J. Chem. Soc., Perkin Trans. 2* **1998**, 2117–2128.
54. (a) Adrian, J. C.; Wilcox, C. S. *J. Am. Chem. Soc*. **1991**, *113*, 678–680. (b) Fielding, L. *Tetrahedron* **2000**, *56*, 6151–6170.

55. Martínez-Díaz, M.-V.; Spencer, N.; Stoddart, J. F. *Angew. Chem., Int. Ed. Engl.* **1997**, *36*, 1904–1907.
56. Although by no means quantitative, the positive-ion FAB mass spectrum of this equilibrium mixture tallies approximately with the ratios of the components observed by ^{1}H NMR spectroscopy in solution. The intensities of the signals in the mass spectrum, corresponding to [**5**·**14**-H·]$^+$:**14**-H$^+$:[**5**·**13**-H]$^+$:**13**-H$^+$, occur in the ratio 100:32:11:5. Signals are not observed for the minor solution components, namely [**5**·**9**-H]$^+$ and **9**-H$^+$, respectively.
57. Fujimori, K.; Yoshimoto, H.; Oae, S. *Tetrahedron Lett*. **1980**, *21*, 3385–3388.
58. Rowan, S. J.; Stoddart, J. F. *Org. Lett*. **1999**, *1*, 1913–1916.
59. The first example of a secondary ammonium ion/binaphthyl-containing crown ether based [2]rotaxane was also prepared using this methodology, see: Cantrill, S. J.; Fyfe, M. C. T.; Heiss, A. M.; Stoddart, J. F.; White, A. J. P.; Williams, D. J. *Chem. Commun*. **1999**, 1251–1252.
60. Amabilino, D. B.; Ashton, P. R.; Pérez-García, L.; Stoddart, J. F. *Angew. Chem., Int. Ed. Engl.* **1995**, *34*, 2378–2380.
61. Thermodynamic control of rotaxane syntheses in a 'statistical' context—by reversible covalent bond formation—has been reported in some earlier investigations. See: ref. 22b and Harrison, I. T. *J. Chem. Soc., Perkin Trans. 1* **1974**, 301–304.
62. Raymo, F. M.; Stoddart, J. F. *Chem. Rev*. **1999**, *99*, 1643–1663.
63. Perrin, D. D.; Armarego, W. F. L. *Purification of Laboratory Chemicals*; Pergamon: Oxford, 1989.
64. Derome, A.; Williamson, M. *J. Mag. Reson.* **1990**, *88*, 177–185.
65. (a) Bax, A.; Davis, D. G. *J. Mag. Reson.* **1985**, *63*, 207–213. (b) Hwang, T.; Shaka, A. J. *J. Am. Chem. Soc.* **1992**, *114*, 3157-3159.
66. Bax, A.; Subramanian, S. *J. Mag. Reson.* **1986**, *67*, 565–569.
67. SHELXTL PC version 5.03, Siemens Analytical X-Ray Instruments, Inc., Madison, WI, 1994.
68. Copies of the crystallographic data can be obtained free of charge on application to CCDC, 12 Union Road, Cambridge CB12 1EZ, UK (Fax: (+44) 1223-336033; E-mail: teched@ccdc.cam. ac.uk).